

1 **Drivers and vertical CO₂ flux balances in a Sahelian *Faidherbia albida* agro-silvo-pastoral**
2 **parkland: Insights from continuous high-frequency soil chamber measurements and**
3 **Eddy Covariance.**

4 Seydina Mohamad Ba ^{a d}, Olivier Roupsard ^{b c d}, Lydie Chapuis-Lardy ^{c f}, Frédéric Bouvery ^g,
5 Yélognissè Agbohessou ^{h i j}, Maxime Duthoit ^{c e}, Aleksander Wieckowski ^k, Torbern Tagesson ^k,
6 Mohamed Habibou Assouma ^l, Espoir K. Gaglo ^{a d}, Claire Delon ^m, Bienvenu Sambou ^a, Dominique
7 Serça ^m

8 ^a Faculté des Sciences et Techniques (FST), Institut des Sciences de l'Environnement (ISE), Université
9 Cheikh Anta Diop (UCAD) de Dakar, 5005, Dakar-Fann, Sénégal

10 ^b CIRAD, UMR Eco&Sols, Dakar, Sénégal

11 ^c Eco&Sols, Univ Montpellier, CIRAD, INRAE, Institut Agro, IRD, Montpellier, France

12 ^d LMI IESOL, Centre IRD-ISRA de Bel Air, Route des hydrocarbures, 18524, Dakar, Sénégal

13 ^e CIRAD, UMR Eco&Sols, Université de Montpellier, Cirad, INRAE, IRD, Institut Agro Montpellier, 2 place
14 Viala, Montpellier, France

15 ^f IRD, UMR Eco&Sols, Université de Montpellier, Cirad, INRAE, IRD, Institut Agro Montpellier, 2 place Viala,
16 Montpellier, France

17 ^g INRAE, 147 rue de l'Université, 75338 Paris, France

18 ^h AIDA, Univ Montpellier, CIRAD, Montpellier, France

19 ⁱ CIRAD, UPR AIDA, Harare, Zimbabwe

20 ^j Department of Plant Production Sciences and Technologies, University of Zimbabwe, Harare, Zimbabwe

21 ^k Department of Physical Geography and Ecosystem Science, Lund University, Sölvegatan 12, S-223 62 Lund,
22 Sweden

23 ^l UMR SELMET, CIRAD, INRAE, Univ Montpellier, Institut SupAgro, Montpellier, France

24 ^m Laboratoire d'Aérodynamique, Université de Toulouse, CNRS, IRD, 14 Avenue Edouard Belin, 31400 Toulouse,
25 France

26 **Corresponding authors:**

27 Seydina Mohamad Ba: seydina.ba@ird.fr

28 Olivier Roupsard: olivier.roupsard@cirad.fr

29 **Highlights:**

- 30 • Long-term high frequency CO₂ flux measurements using automated static
31 chambers in a Sahelian *F. albida* parkland.
- 32 • Empirical gap-filling and flux partitioning methods validated against Eddy
33 Covariance GPP.
- 34 • Fluxes peaked during the rainy season both at a distance from trees in full sun (FS)
35 and under tree canopies (Sh), driven mainly by soil moisture and leaf area.
- 36 • *F. albida* trees enhance CO₂ fluxes under canopies ("fertile island" effect) and
37 account for ~23% of annual ecosystem GPP.

38 **ABSTRACT:**

39 Agroforestry systems — combining trees with crops and/or livestock — are increasingly
40 promoted as sustainable and climate-resilient land-use strategies. Despite their widespread
41 presence in the Sahel, experimental data on their potential as carbon sinks are scarce. This study
42 presents a full-year, high-frequency dataset of CO₂ fluxes in a Sahelian agro-silvo-pastoral
43 parkland dominated by *Faidherbia albida*, located in Senegal's groundnut basin. CO₂ fluxes were
44 continuously measured using automated static chambers, allowing the quantification of soil and
45 crop respiration (R_{ch}), gross primary production (GPP_{ch}), and net carbon exchange (FCO_{2ch})
46 under both full sun and shaded (under tree canopies) environments. Seasonal patterns of CO₂
47 fluxes were similar in both environments, with peaks during the rainy season. R_{ch} and GPP_{ch}
48 were significantly higher under tree canopies, indicating a 'fertile island' effect. CO₂ flux variability
49 was primarily driven by soil moisture and leaf area index. Chamber-based GPP estimates closely
50 matched those from Eddy Covariance measurements. On an annual scale, *F. albida* trees
51 contributed approximately 23% of total ecosystem GPP, with a carbon use efficiency of 0.48. Net
52 annual vertical CO₂ exchange was estimated at -1.4 ± 0.46 and -1.8 ± 0.17 Mg C-CO₂ ha⁻¹ using
53 chamber and Eddy Covariance methods, respectively. These findings underscore the role of *F.*
54 *albida*-based agroforestry systems as effective carbon sinks in Sahelian landscapes, supporting
55 their potential contribution to climate change mitigation.

56 **Keywords:** Sahelian agro-silvo-pastoral systems, CO₂ fluxes, automated static chambers, Eddy
57 Covariance, 'fertile island effect', carbon balances.

58 1. Introduction

59 Plant photosynthesis and respiration —both autotrophic (plant) and heterotrophic (microbial)—
60 are fundamental processes driving carbon dioxide (CO₂) fluxes in terrestrial ecosystems
61 (Lambers et al., 2008; Raich et al., 2014; Reichle, 2020). Accurate quantification of these processes
62 is critical for assessing ecosystem carbon (C) sink potential (Baldocchi, 2020), particularly for
63 informing climate-smart land management strategies.

64 To capture these processes at the ecosystem scale, the Eddy Covariance (EC) technique has
65 emerged as a transformative method, enabling continuous and high-frequency CO₂ flux
66 measurements (Baldocchi, 2003, 2008). The EC technique quantifies CO₂ exchanges between
67 ecosystems and the atmosphere by correlating fluctuations in vertical wind velocity with
68 simultaneous variations in CO₂ concentrations, providing a direct and non-invasive estimate of
69 CO₂ fluxes (Baldocchi, 2003). Extensive EC networks in Europe (Stojanović et al., 2024), Asia (Yu
70 et al., 2011), and the Americas (Chu et al., 2021) have significantly advanced our understanding
71 of the global C cycle. In contrast, sub-Saharan Africa remains critically underrepresented
72 (Bombelli et al., 2009; Houghton & Hackler, 2006; Williams et al., 2007). Although some studies
73 have used EC (Ardö et al., 2008; Brümmer et al., 2008; Merbold et al., 2009; Tagesson et al., 2016),
74 static chambers (Assouma et al., 2017; Owusu et al., 2024; Rosenstock et al., 2016; Wachiye et al.,
75 2020), or modeling approaches (Agbohessou et al., 2023, 2024; Delon et al., 2019; Rahimi et al.,
76 2021), they remain sparse and methodologically heterogeneous, limiting comparability and
77 regional C budget integration.

78 Among these underrepresented landscapes, agroforestry systems in the Sahel— particularly
79 agro-silvo-pastoral systems (ASPS) that combine trees, crops, and livestock— are increasingly
80 promoted for sustainable land management and climate resilience (Cardinael et al., 2021; Gupta
81 et al., 2023; Mbow et al., 2014; Stetter & Sauer, 2024). However, the structural and functional
82 heterogeneity of these systems poses significant challenges for accurately quantifying and
83 upscaling C fluxes. *Faidherbia albida*, a keystone agroforestry tree species in these ASPs (Leroux
84 et al., 2022; Lu et al., 2022), is of particular interest due to its reverse phenology, capacity to
85 enhance soil fertility and crop yields (Bayala et al., 2020; Roupsard et al., 2020; Sileshi et al., 2016;
86 2020). Yet, its functional role in modulating both the magnitude and seasonal dynamics of CO₂
87 fluxes remains poorly understood.

88 Addressing this knowledge gap requires integrated approaches capable of capturing both
89 aggregate and component-specific CO₂ fluxes. While EC remains the gold standard method for CO₂
90 flux measurements at the landscape scale (Baldocchi, 2003), it captures net ecosystem exchange
91 (NEE) as an aggregate signal, without separating the contributions from individual compartments
92 such as soil, crops, and trees. This limits its utility for disentangling processes and attributing
93 sources in heterogeneous systems like ASPs. Automatic static chambers provide a valuable

94 complement to EC, as they enable continuous, high-frequency measurements at finer scales and
95 at the level of specific ecosystem components. This approach facilitates component-specific
96 quantification of CO₂ fluxes, particularly from soil and crop compartments (Luo & Zhou, 2006;
97 Denmead, 2008; Zaman et al., 2021). When combined with EC, this dual-method approach
98 strengthens source attribution and improves the partitioning of fluxes across complex
99 agroforestry landscapes.

100 This study presents one of the first integrated quantification of CO₂ fluxes in a Sahelian ASPS
101 dominated by *F. albida*, combining EC and automatic static chambers.

102 Specifically, the study aims to (1) conduct year-round, high-frequency *in situ* CO₂ flux
103 measurements from soil and crops using automated static chambers; (2) partition the net CO₂
104 fluxes (FCO₂ch) into respiration (Rch) and photosynthesis (GPPch); (3) investigate the
105 environmental drivers of fluxes and the spatial variability linked to tree presence; and (4)
106 compare chamber-based flux estimates with ecosystem-scale measurements derived from the EC
107 method.

108 Based on these objectives, we hypothesize that (1) Rch and GPPch are higher under the canopy of
109 *F. albida* than in full sun, (2) soil moisture is the main environmental factor directly controlling
110 both Rch and GPPch, (3) when extrapolated to the field scale, the chamber-based method provides
111 seasonal dynamics of respiration and photosynthesis fluxes comparable to those derived from EC
112 technique.

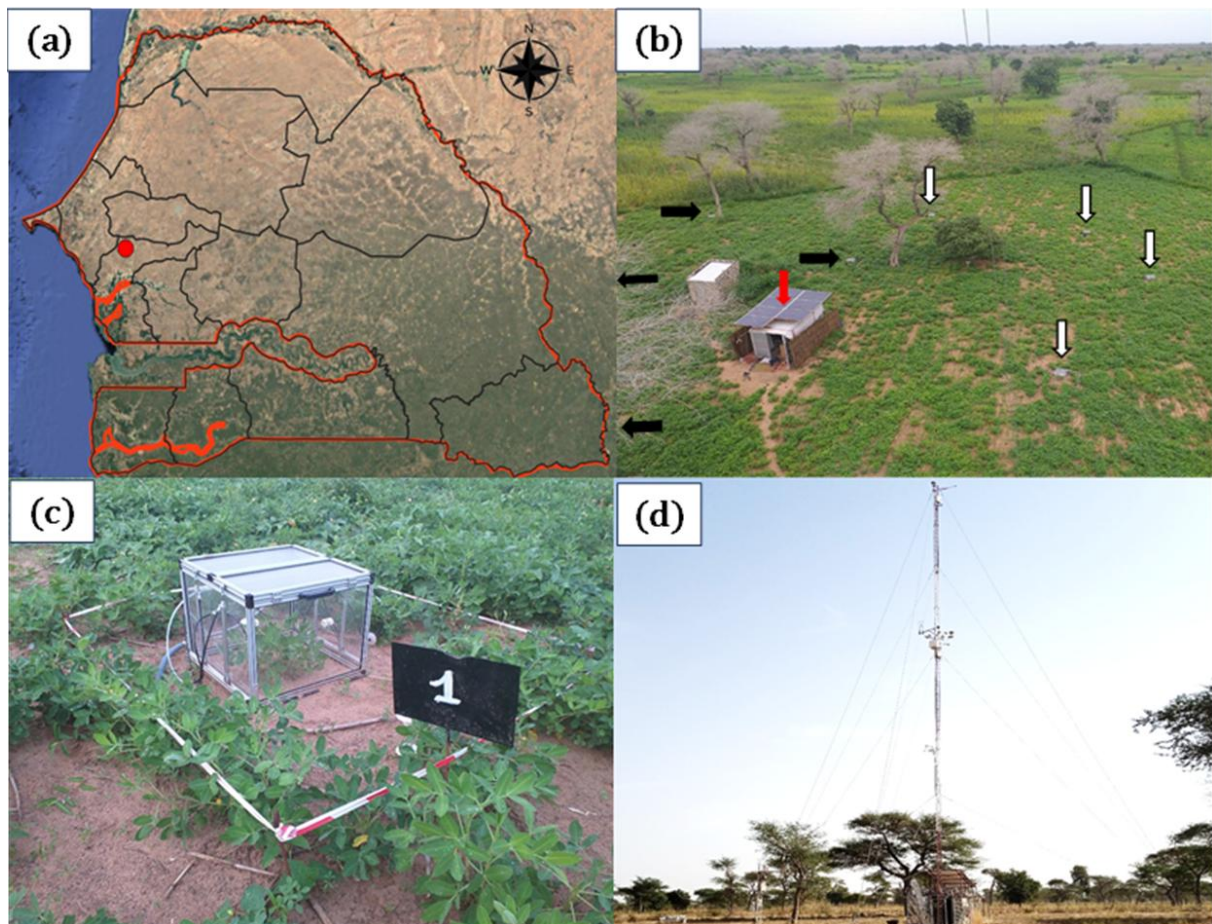
113 2. Materials and methods

114 2.1. Site description

115 The study was conducted in the agroforestry parkland of Sob village (Niakhar municipality, Fatick
116 region), located in the groundnut basin of Senegal, within the Sahelo-Sudanian climatic zone of
117 West Africa (Fig. 1). The climate is characterized by a long dry season (8–9 months) with high
118 temperatures and strong diurnal variations, and a short rainy season from late June to mid-
119 October (Delaunay et al., 2018).

120 Soils are locally known as “*Dior*” and classified as Arenosols (IUSS Working Group WRB, 2022).
121 The topsoil has low organic matter (<1%) and phosphorus (<3 mg kg⁻¹), a sandy texture (>85%
122 sand), and an acidic pH (Malou et al., 2021; Siegwart et al., 2022). Rainfed agriculture
123 predominates. The main cropping system includes pearl millet (*Pennisetum glaucum L.*) and
124 groundnut (*Arachis hypogaea L.*) in biennial rotation, with occasional intercropping of cowpea
125 (*Vigna unguiculata L.*).

126 The site hosts the 'Faidherbia Flux' station (14°29'44.916"N; 16°27'12.851"W; FLUXNET ID: SN-
127 Nkr), a long-term research platform for monitoring ecosystem services in agroforestry systems.
128 It is dominated by *F. albida*, a nitrogen-fixing, reverse-phenology tree with deep roots accessing
129 groundwater (Roupsard et al., 1999). The tree density is ~13 trees ha⁻¹, with canopies covering
130 ~10% of the soil surface (Roupsard et al., 2020). The EC tower is installed at 20 m height,
131 approximately 12.5 m above the canopy. The study field is a typical 'bush field', characterized by
132 low soil fertility, no mineral fertilization, and off-site export of crop residues and manure (Malou
133 et al., 2021).



134 Fig. 1: Study area.

135 (a) geographical location of Sob, Groundnut basin, Senegal (Map data © Google Earth, 2025), (b) overview
 136 (image from the Eddy Covariance tower located in the same bush-field) of the *Faidherbia albida* parkland
 137 during the rainy season, depicting groundnut crops with bare soil in the inter-row, *F. albida* trees
 138 (defoliated during the rainy season, average height = 13m) and location of the chambers under the Shade
 139 of trees (horizontal black arrows; N=4) and in Full sun (vertical white arrows; N=4); The shelter (red
 140 arrow) with solar panels is to fit the analyser, automation and batteries (c) automatic chamber enclosing a
 141 groundnut plant (during the rainy season) or bare soil (during the dry season), (d) Eddy Covariance (EC)
 142 tower (measurement height = 20 m) during the dry season.

143 *2.2. Experimental setup*

144 *2.2.1. CO₂ flux measurements in automatic chambers*

145 Continuous net CO₂ fluxes (FCO₂ch) from soil and groundnut plants were measured over a full
146 phenological year (June 17, 2021 – June 17, 2022) using eight automated static chambers
147 (50×50×50 cm), each enclosing one groundnut plant. Four chambers were installed in full sun
148 (FS), at least 20 m from trees, and four under *F. albida* canopy shade (Sh). The chambers were
149 transparent, custom-built (Duthoit et al., 2020), and installed on metal bases embedded 10 cm
150 into the soil one month prior to measurements.

151 During the rainy season (June–November), groundnut coexisted briefly with spontaneous weeds
152 until weeding (mid-July), after which chambers contained only groundnut. Post-harvest (early
153 November), chambers remained bare while surrounding plots experienced weed regrowth.

154 CO₂ concentrations were measured at 1 Hz using a Picarro G2508 gas analyser (Picarro Inc., Santa
155 Clara, CA, USA) (Fleck et al., 2013; Reum et al., 2019; Valujeva et al., 2022). A fully automated
156 system was built for sequential half-hour flux measurements alternating FS and Sh chambers
157 (Table S2). Measurement duration was 15 min per chamber in the dry season, reduced to 5 min
158 during the rainy season to limit condensation effects.

159 *2.2.2. CO₂ flux measurements by Eddy Covariance*

160 The EC system (Li-COR SMARTFLUX®, including a Gill MasterPro 3D sonic anemometer and a LI-
161 7500 RS open path CO₂ and H₂O gas analyser) was mounted at a height of 20 m on a 30m mast,
162 above *F. albida*. It continuously monitored net CO₂ exchange from the ecosystem. Raw data were
163 collected at 20 Hz frequency and post-processed from binary files using the advanced mode of the
164 EddyPro® v7.0, with standard corrections and procedures: sonic tilt correction (double rotation),
165 block averaging, covariance maximisation for time lag, and WPL correction (Webb et al., 1980).
166 Quality control followed Foken et al. (2004) and Vickers & Mahrt (1997); random uncertainty was
167 estimated per Finkelstein & Sims (2001). Spectral corrections were applied according to
168 Moncrieff et al. (1997, 2004). Footprints were computed according to Kormann and Meixner
169 (2001), using the FREddyPro R package (Xenakis, 2016), indicating a ~1 ha source area covering
170 the entire field. Gap-filling and flux partitioning were conducted using ReddyProc (Wutzler et al.,
171 2018), applying the daytime partitioning approach of Lasslop et al. (2010).

172 *2.2.3. Ancillary measurements*

173 Environmental and vegetation variables were monitored continuously throughout the study.
174 Global radiation (Rg) was estimated from photosynthetically active radiation (PAR) using a Skye
175 sensor (averaged over 30-min intervals). The normalised difference vegetation index (NDVI) of

176 crops under full sun was recorded semi-hourly by a calibrated downward-facing sensor installed
177 at 20 m height (Pontauiller et al., 2003), processed following Soudani et al. (2012), and used to
178 estimate the leaf area index (LAI) time series for groundnut, weeds, and cowpea based on end-of-
179 season field LAI measurements in six 15 m² plots (as in Roupsard et al., 2020).

180 Rainfall was recorded by an automatic weather station (CR1000 with TE525MM rain gauge,
181 Campbell Scientific), and soil volumetric water content (VWC) and temperature (T_{soil} , at 6 cm
182 depth) were monitored using TOMST® TMS-4 sensors, benchmarked prior to field deployment
183 inside and outside the chambers (Wild et al., 2019). Air temperature (T_{air}) was recorded inside
184 each chamber at 15 cm above ground, all at 5-min intervals. These measurements contribute to
185 the SoilTemp global database (Lembrechts et al., 2020, 2022).

186 Groundnut development was tracked weekly by counting leaves in each chamber. Total
187 groundnut LAI (LAI_{ch}) was then derived from average single-leaf area and chamber surface.

188 A detailed description of the data used in this study is provided in Supplement (Table S1).

189 *2.3. Data processing*

190 *2.3.1. Flux calculation*

191 Net CO₂ fluxes (FCO₂ch, in μmol CO₂ m⁻² s⁻¹) from the chambers were calculated from the linear
192 change in CO₂ concentration over time ($\Delta C/\Delta t$; Fig. S1 and Fig. S2) using the Eq.1.

$$193 \text{FCO}_{2\text{ch}} = \left(\frac{P}{RT_k}\right) \left(\frac{V}{A}\right) \left(\frac{\Delta C}{\Delta t}\right) \quad (\text{Eq. 1})$$

194 where P is atmospheric pressure (101 325 N m⁻²), R is the ideal gas constant (8.31 N m mol⁻¹ K⁻¹),
195 T_k is air temperature inside the chamber in Kelvin, V (0.125 m³) is the total system volume
196 (chamber, tubing, analyser cavity, pump, and water trap), and A (0.25 m²) is the chamber
197 footprint. The slope $\Delta C/\Delta t$ was obtained via linear regression (Duthoit et al., 2020).

198 Mean FCO₂ch values were computed separately for the four replicate chambers in full sun (FS)
199 and under *F. albida* shade (Sh). By convention, negative values indicate net CO₂ uptake
200 (photosynthesis), and positive values indicate net CO₂ release (respiration).

201 *2.3.2. Quality control of chamber-based CO₂ flux measurements*

202 The quality of chamber-based CO₂ flux measurements was assessed using a threshold of $R^2 \geq 0.8$
203 of the linear increase in CO₂ concentration during chamber closure. The minimum detectable flux
204 (MDF) was then calculated following Nickerson (2016) (Eq.2). The MDF defines the flux detection
205 threshold, below which data are considered unreliable due to instrument sensitivity and sampling
206 constraints (Zaman et al., 2021). In this study, the MDF was ± 0.0004 μmol CO₂ m⁻² s⁻¹.

207
$$\mathbf{MDF} = \left(\frac{A_a}{tc(\sqrt{tc/ps})} \right) \left(\frac{VP}{ART} \right) \quad (\mathbf{Eq. 2})$$

208 where A_a is the analytical precision of the Picarro analyser (0.6 ppm; Picarro Inc., 2015), tc the
 209 closure time (s), p_s the sampling frequency (1 Hz), V the chamber volume, P the atmospheric
 210 pressure (101 325 N m⁻²), A the chamber footprint, R the gas constant (8.3 N m mol⁻¹·K⁻¹), and T
 211 the air temperature in Kelvin.

212 Following this quality control, fluxes were partitioned (Section 2.3.3) and gap-filled (Section
 213 2.3.4).

214 *2.3.3. Partitioning of chamber-based CO₂ fluxes*

215 The net CO₂ fluxes (FCO₂ch), averaged from four chambers per environment (FS and Sh), were
 216 partitioned into two components according to Eq. 3 (Reichstein et al., 2005).

217
$$\mathbf{FCO_2ch} = \mathbf{Rch} + \mathbf{GPPch} \quad (\mathbf{Eq. 3})$$

218 Rch includes heterotrophic respiration (Rh) from soil and other autotrophic respiration (Ra) from
 219 groundnut plants and roots of *F. albida* (Ra Groundnut + Ra tree below-ground). Rch is always
 220 positive (Rch > 0). GPPch (Gross Primary Productivity) represents the photosynthetic CO₂ uptake
 221 by the groundnut plants and is negative during the day (GPPch < 0), and zero at night, when
 222 FCO₂ch = Rch.

223 Half-hourly FCO₂ch fluxes were partitioned as follows: (1) an Arrhenius-type function (Lloyd &
 224 Taylor, 1994) was fitted between nocturnal Rch and T_{soil} during nighttime periods, for each 5-days
 225 throughout the time series (Eq. 4). This empirical formulation is based on several key
 226 assumptions. First, the relationship between nocturnal respiration and soil temperature is
 227 assumed to follow an exponential response, reflecting the temperature sensitivity of respiration
 228 processes. Second, the model assumes temporal stability of the respiration-temperature
 229 relationship between night and day, allowing diurnal respiration to be extrapolated from fitted
 230 parameters in Eq.4 and daytime T_{soil}. Third, we assumed that no abrupt changes in substrate
 231 availability or soil moisture occur between day and night — conditions that could otherwise
 232 disrupt the temperature-respiration relationship. These assumptions are widely applied in CO₂
 233 flux partitioning approaches (Reichstein et al., 2005; Lasslop et al., 2010). (2) Diurnal Rch was
 234 estimated by applying the Lloyd & Taylor function, previously calibrated on nocturnal data, to the
 235 corresponding daytime T_{soil} measurements for each 5-day interval. (3) GPPch was subsequently
 236 derived as the residual component of the net CO₂ flux during the day, according to:

237 **nocturnal Rch** = $R_{\text{ref}} \cdot \exp \left[E_0 \left(\frac{1}{T_{\text{ref}} - T_0} - \frac{1}{T_{\text{soil}} - T_0} \right) \right]$ (Eq. 4)

238 where R_{ref} ($\mu\text{mol CO}_2 \text{ m}^{-2} \text{ s}^{-1}$) is a fitted parameter representing the base respiration at the
 239 reference temperature [T_{ref} (K), (set at 288.15 K)]. E_0 (K) is the temperature sensitivity (set at
 240 250 K), T_{soil} (K) the soil temperature (K), and T_0 (K) is kept constant at 231.13 K, according to
 241 Lloyd & Taylor (1994).

242 **GPPch** = **diurnal FCO₂ch** – **diurnal Rch** (Eq. 5)

243 where diurnal FCO₂ch and diurnal Rch represent the daytime net CO₂ fluxes and respiration in
 244 $\mu\text{mol CO}_2 \text{ m}^{-2} \text{ s}^{-1}$, respectively.

245 2.3.4. Gap-filling procedure

246 Missing Rch data were gap-filled using the model derived from Eq. 4 (Lloyd & Taylor, 1994). Prior
 247 to gap-filling GPPch, raw data were standardised by LAI to reduce variability between chambers
 248 due to differences in leaf surface area (Eq. 6). A light-response model was then fitted to the
 249 standardised GPPch data, every 5-day period, to gap-fill missing values. The model is based on a
 250 rectangular hyperbolic function that describes the relationship between photosynthetic CO₂
 251 uptake and incoming global radiation (Rg) (Eq. 7). It corresponds to a Michaelis–Menten-type
 252 light-response curve, commonly used in ecosystem carbon exchange studies (Falge et al., 2001;
 253 Lasslop et al., 2010).

254 **GPPch.stand** = $\frac{\text{GPPch}}{\text{LAIch}} * \text{LAI.field}$ (Eq. 6)

255 where GPPch.stand ($\mu\text{mol CO}_2 \text{ m}^{-2} \text{ s}^{-1}$) is the standardised GPPch. LAI_{ch} and LAI_{field} ($\text{m}^2 \text{ leaves}$
 256 $\text{m}^{-2} \text{ soil}$) represent the groundnut LAI inside the chambers and the groundnut + weeds + cowpea
 257 LAI for the whole field, respectively.

258 **GPP** = $\frac{\alpha\beta Rg}{\alpha Rg + \beta}$ (Eq. 7)

259 where α ($\mu\text{mol CO}_2 \text{ J}^{-1}$) represents the light use efficiency of the groundnut plants inside the
 260 chambers, and refers to the initial slope of the light-response curve, β ($\mu\text{mol CO}_2 \text{ m}^{-2} \text{ s}^{-1}$) is the
 261 maximum CO₂ uptake rate by the groundnut plants at light saturation, and Rg the global radiation
 262 (W m^{-2}).

263 2.3.5. Comparing chamber-based (Ch) and Eddy Covariance (EC) methods

264 Chamber measurements were upscaled to field-level CO₂ fluxes and compared with EC-derived
 265 fluxes. Before comparison, a correction was applied (Eq. 6) to account for differences in LAI
 266 between chambers (LAI_{ch}) and the field (LAI_{field}), due to the presence of cowpea and weeds in
 267 the field but not in the weeded chambers.

268 Upscaling considered tree cover, with FS and Sh chamber fluxes weighted at 90% and 10%,
 269 respectively. Rch.stand and GPPch.stand, representing chamber-based respiration and

270 photosynthesis at field scale. These fluxes were compared, on a half-hourly basis, to EC-derived
271 Reco.EC and GPP.EC (Table S4). The November–December transition period was excluded due to
272 weed-driven uncertainties after groundnut harvest.

273 During the rainy season (*F. albida* leafless), GPP.EC represented ground vegetation (groundnut,
274 cowpea, weeds), while Reco.EC included autotrophic respiration from all vegetation (including
275 trees), and heterotrophic respiration (Reco.EC = R_a tree below-ground + R_a tree above-ground
276 + R_a groundnut + R_a cowpea + R_a weeds + R_h). Rch.stand could not be fully upscaled to the field
277 due to uncertainty in its partitioning between R_a and R_h . Rch.stand accounted only for R_a tree
278 below-ground, R_a groundnut, and R_h .

279 In the dry season (leafy trees, bare soil), GPP.EC reflected tree photosynthesis only (GPP tree),
280 while GPPch.stand was nil. Reco.EC included R_a tree (above- and below-ground) and R_h .
281 Rch.stand, measured on bare soil, represented only R_a tree below-ground + R_h .

282 *2.3.6. Contribution of trees to full ecosystem respiration and photosynthesis*

283 During the dry season, when the trees (*F. albida*) maintained their foliage, a comparison between
284 chamber and EC measurements allowed for the estimation of the contribution of the above-
285 ground tree compartments to total ecosystem respiration (Table S4). Based on this estimate, total
286 tree respiration (R_a tree) was then calculated under the assumption that the tree root systems
287 (R_a tree below-ground) represent $\frac{1}{3}$ of the above-ground biomass (Jackson et al. 1996).

288 Given the GPP measured during the dry season was equivalent to GPP of trees (GPP trees) from
289 EC measurements, the carbon use efficiency of the trees (CUE tree) was then calculated (Table
290 S4). The resulting CUE value was assessed to determine whether it approximated the typical value
291 of 0.5, which is often used as a default in ecosystem models (Zhou et al., 2019; 2020).

292 *2.3.7. Net annual vertical C balance at the ASPS scale*

293 The net C balance of CO₂ fluxes in a yearly basis was estimated for chambers and EC measurements
294 in Mg C-CO₂ ha⁻¹. The chambers CO₂ flux balances were obtained by calculating the annual sum
295 of the net CO₂ flux measurements and then weighting with the tree cover rate (10% for the Sh,
296 90% for the FS). These annual balances for the field are considered apparent representing vertical
297 CO₂ exchanges only, as they do not account for the biomass exported from the field after the
298 harvest, the decomposition of which therefore escaped both the chambers and the EC.
299 Additionally, the inputs and the outputs of faecal matter resulting from livestock wandering
300 during the dry season were not quantified and are therefore neglected. The objective here is to
301 compare two approaches at different scales using vertical net C balances, rather than to provide
302 an absolute C budget which would also include horizontal transfers of carbon.

303 2.4. Statistical analyses

304 Statistical analyses were performed using the R software (R. Core Team, 2023). To compare the
305 mean values of climatic parameters between the FS and Sh situations, a non-parametric Mann-
306 Whitney test was used when both the normality (`shapiro.test`) and the homogeneity of the
307 variance (Levene Test, R package 'Car'; Fox et al., 2023) were not confirmed. This approach was
308 similarly applied to compare the seasonal dynamics of CO₂ fluxes between FS and Sh, as well as
309 between the chamber-based and Eddy Covariance (EC) methods. Means and standard deviations
310 were computed using the 'skim' function from the R package 'skimr' (Waring et al., 2022).

311 Respiration (R_{ch}) (Eq. 4) and GPP (GPP_{ch}) models (Eq. 7) were fitted using non-linear least
312 squares regression, implemented in the library in R 'nls.multstart' (Padfield et al., 2025). For the
313 GPP_{ch} model, parameters α and β with non-significant p-values were removed, and then the
314 remaining values were interpolated and smoothed using a 'spline' function from the 'zoo' library
315 in R (Zeileis et al., 2024). Ordinary least-square linear regressions were fitted between the
316 measured and the modeled values derived from. Model performance of Eq. 4 and Eq. 7 was
317 evaluated by fitting ordinary least-square linear regressions between the measured and the
318 modeled values using R², root mean square error (RMSE), and the bias metrics. Given that the
319 primary objective of these equations was to accurately reproduce the seasonal dynamics of the
320 CO₂ fluxes to fill gaps in data, particular emphasis was placed on R², with a higher value reflecting
321 a better fit of the model to the measurements.

322 Correlation analysis was conducted between chamber CO₂ fluxes (FCO_{2ch}, R_{ch}, GPP_{ch}) and soil
323 temperature (T_{soil}, °C), air temperature (T_{air}, °C), VWC, the leaf area index of groundnut plants in
324 the chambers (LAI_{ch}), and the fitted parameters for respiration — R_{ref} — and photosynthesis —
325 α and β . This analysis was performed using the 'cor.test' function from the 'stats' package in R
326 (Lüdecke et al., 2021), applying the Spearman method.

327 The threshold of the daily mean soil temperature (T_{soil}, °C) at which the cumulative daily
328 respiration (R_{ch}, g C-CO₂ m⁻² d⁻¹) began to decline was determined using segmented regression
329 from the R package 'segmented' (Muggeo, 2003). The associated uncertainty (standard error) of
330 this estimate was evaluated through a bootstrap procedure.

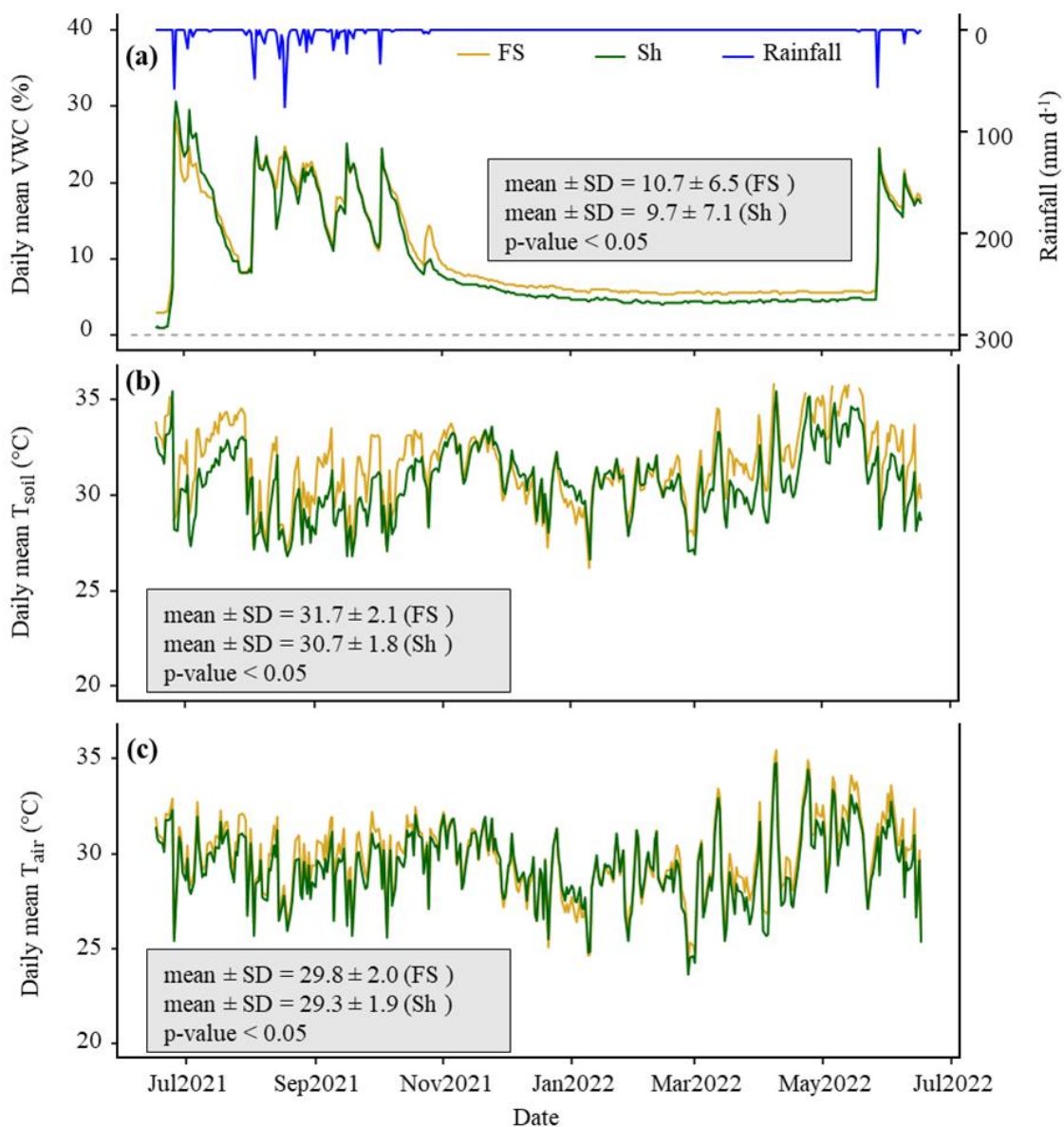
331 The standard error of the total annual flux was estimated using the error propagation method.
332 This calculation considered the mean standard deviation of daily fluxes (g C-CO₂ d⁻¹) and the
333 effective number of measurement days (365). For each FS and Sh condition, the mean daily
334 standard deviation was multiplied by the square root of 365 to obtain the annual standard error.
335 The resulting values were then weighted by 90% for FS and 10% for Sh to derive the overall
336 standard error of the annual flux sum, which was subsequently converted to Mg C-CO₂ ha⁻¹.

337 3. Results

338 3.1. Microclimatic conditions

339 During the experiment, the cumulative rainfall was 550 mm, which was representative of the
340 interannual average. Precipitations were lowest in July and highest between August and
341 September, a period that typically corresponds to the peak of the rainy season (Fig. 2a). Global
342 radiation ranged between 5.8 and 32.4 MJ m⁻² d⁻¹ (data not shown). The daily mean VWC in the
343 chambers showed significant variation, ranging from 1% at the end of the dry season to a
344 maximum of 30% during the rainy season (Fig. 2a). While VWC was similar during the rainy
345 season, it remained consistently higher in FS than in Sh throughout the dry season ($p < 0.05$),
346 which was unexpected. However, it should be noted that the last rain of October 2021 recharged
347 the FS chambers more effectively, likely due to foliage rainfall interception by *F. albida* which had
348 just put on leaves at that time, potentially explaining this discrepancy in VWC.

349 Within the chamber, the daily mean T_{soil} ranged from 26°C in April to 37.5°C at the end of the dry
350 season (Fig. 2b), while T_{air} varied between 23.7°C and 35.5°C (Fig. 2c). However, during
351 instantaneous daily peaks, T_{soil} could exceed 45°C in May (data not shown). As expected, both daily
352 mean T_{soil} and T_{air} were significantly higher in FS compared to Sh situations ($p < 0.05$), with T_{soil}
353 and T_{air} averaging respectively 1°C and 0.5°C lower under the tree canopy.



354 Fig. 2: One-year time series of daily average microclimatic parameters measured inside the
 355 chambers.

356 (a) volumetric soil water content (VWC) at a depth of 6 cm (%). (b) soil temperature (T_{soil}) at a depth of 6
 357 cm ($^{\circ}\text{C}$), (c) air temperature (T_{air}) at a height of 15 cm ($^{\circ}\text{C}$). The blue line depicts the daily rainfall (mm d^{-1})
 358 throughout the year. FS: Full sun chambers; Sh: Shaded chambers. Mean and SD represent respectively the
 359 mean value and the standard deviation. The p-value indicates the probability associated with the statistical
 360 test, assessing the differences in means between FS and Sh with the significance level α set to 0.05.

361 *3.2. Modeling the chamber-based total respiration (R_{ch}) and photosynthesis (GPP_{ch})*

362 *3.2.1. Dynamics of reference respiration, light use efficiency, and maximum CO₂ uptake rate at*
363 *light saturation (R_{ref}, α , and β)*

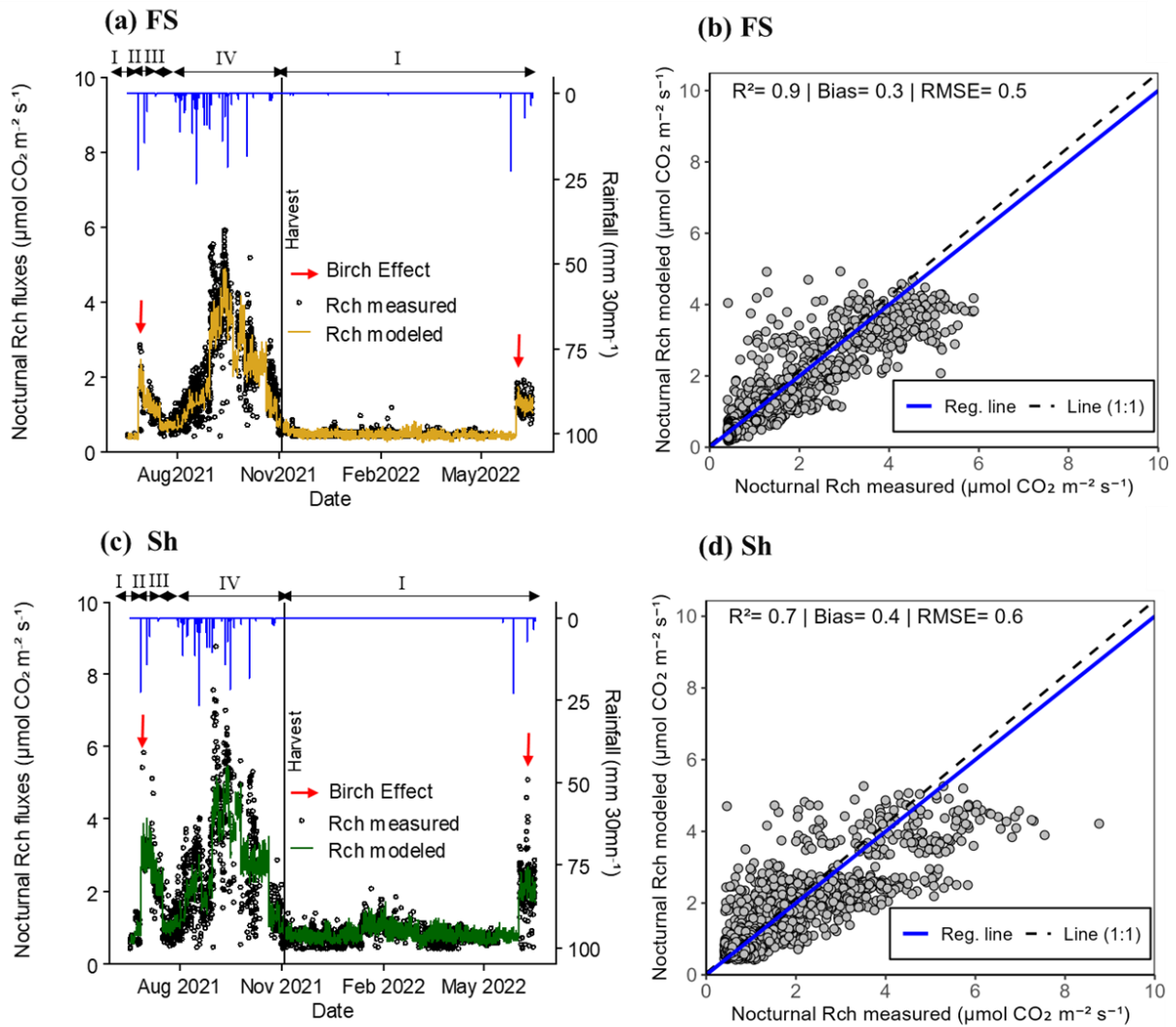
364 The reference respiration (R_{ref}) showed comparable seasonal dynamics both at a distance from
365 the trees (FS) and under the tree canopies (Sh) (Fig. S4). In both situations, R_{ref} showed strong
366 variability during the rainy season, peaking in September 2021 at 2.4 $\mu\text{mol CO}_2 \text{ m}^{-2} \text{ s}^{-1}$ for FS and
367 2.9 $\mu\text{mol CO}_2 \text{ m}^{-2} \text{ s}^{-1}$ for Sh (Table S3). In contrast, during the dry season — from November 3,
368 2021 (after harvest) until the onset of the following rainy season (June 2022) — R_{ref} values
369 dropped both for FS and Sh, averaging $0.3 \pm 0.5 \mu\text{mol CO}_2 \text{ m}^{-2} \text{ s}^{-1}$ for FS and $0.5 \pm 0.6 \mu\text{mol CO}_2$
370 $\text{m}^{-2} \text{ s}^{-1}$ for Sh. This represents a reduction by a factor of 8 for FS and 6 for Sh compared to the
371 rainy season. The mean annual R_{ref} values were significantly higher under Sh than in FS, with value
372 approximately 1.5 times greater (Table S3).

373 Regarding GPP in chambers, the light use efficiency (α) and the maximum CO₂ uptake by
374 groundnut plants in the chambers (β), also reached their maximum during the peak of the rainy
375 season (Fig. S5, a and b). The maximum value of α reached 0.2 $\mu\text{mol CO}_2 \text{ J}^{-1}$ in FS and 0.3 μmol
376 $\text{CO}_2 \text{ J}^{-1}$ in Sh (Table S3). Similarly, the maximum values of optimum CO₂ uptake rate at light
377 saturation (β) were 40.2 $\mu\text{mol CO}_2 \text{ m}^{-2} \text{ s}^{-1}$ for FS and 42.8 $\mu\text{mol CO}_2 \text{ m}^{-2} \text{ s}^{-1}$ for Sh (Table S3). In
378 the dry season, when photosynthetic activity ceased in the chambers, both α and β were assumed
379 to be nil (Fig. S5, a and b). On average, α and β were significantly higher in Sh than in FS, by a factor
380 of 1.7 and 1.2, respectively (Table S3). We noted that the decline in photosynthetic activity of the
381 groundnut crop occurred earlier and rapidly at a distance from the trees (FS), as reflected by the
382 sharply observed recession of α and β in FS.

383 *3.2.2. Dynamics of nocturnal respiration in chambers*

384 The averaged nocturnal respiration (nocturnal R_{ch}) calculated from the measurements across
385 each treatment (FS and Sh), showed similar seasonal patterns (Fig. 3, a and c). Following the first
386 rains, R_{ch} values increased dramatically, with a nocturnal 'Birch effect' — a sudden pulse of CO₂
387 release following soil rewetting — observed to be more pronounced under Sh compared to FS,
388 approximately by a factor of 2. At the peak of the rainy season (September), the maximum
389 nocturnal R_{ch} values reached approximately 6.0 $\mu\text{mol CO}_2 \text{ m}^{-2} \text{ s}^{-1}$ in FS and 9.0 $\mu\text{mol CO}_2 \text{ m}^{-2} \text{ s}^{-1}$
390 in Sh (Fig. 3, a and c). Thereafter, nocturnal R_{ch} declined well before the groundnut harvest along
391 with the rainfall spacing and the groundnut crop senescence (data not shown). During the dry
392 season nocturnal R_{ch} continued to decrease, with maximum values around 1.0 $\mu\text{mol CO}_2 \text{ m}^{-2} \text{ s}^{-1}$
393 in FS and 2.0 $\mu\text{mol CO}_2 \text{ m}^{-2} \text{ s}^{-1}$ in Sh (Fig. 3, a and c).

394 The modeled nocturnal Rch values closely matched the measured nocturnal Rch values (mean
395 across four chambers per treatment), as indicated by the model performance metrics ($R^2 = 0.9$,
396 with bias and RMSE values of 0.3 and 0.5 $\mu\text{mol CO}_2 \text{ m}^{-2} \text{ s}^{-1}$, respectively, for FS; $R^2 = 0.7$, with bias
397 and RMSE values of 0.4 and 0.6 $\mu\text{mol CO}_2 \text{ m}^{-2} \text{ s}^{-1}$, respectively, for Sh) (Fig. 3, b and d). Similarly,
398 the daily mean modeled values also fitted well with the measured values, with FS showing (mean
399 \pm standard deviation) $0.9 \pm 0.9 \mu\text{mol CO}_2 \text{ m}^{-2} \text{ s}^{-1}$ (modeled) and $1.2 \pm 1.2 \mu\text{mol CO}_2 \text{ m}^{-2} \text{ s}^{-1}$
400 (measured), while Sh recorded $1.4 \pm 0.9 \mu\text{mol CO}_2 \text{ m}^{-2} \text{ s}^{-1}$ (modeled) and $1.5 \pm 1.2 \mu\text{mol CO}_2 \text{ m}^{-2}$
401 s^{-1} (measured). Given the close match between the measured and modeled values, the fitted
402 model parameters were used subsequently to fill data gaps and estimate diurnal Rch values, as
403 presented in Fig. 4, a and c.



404 Fig. 3: Dynamics of instantaneous nocturnal CO₂ fluxes in chambers in Full sun (FS; a and b) and
 405 Shaded (Sh; c and d) environments (data filtered based on R² of the CO₂ variation over the time
 406 of chamber closure and Minimum Detectable Flux, Eq.2).

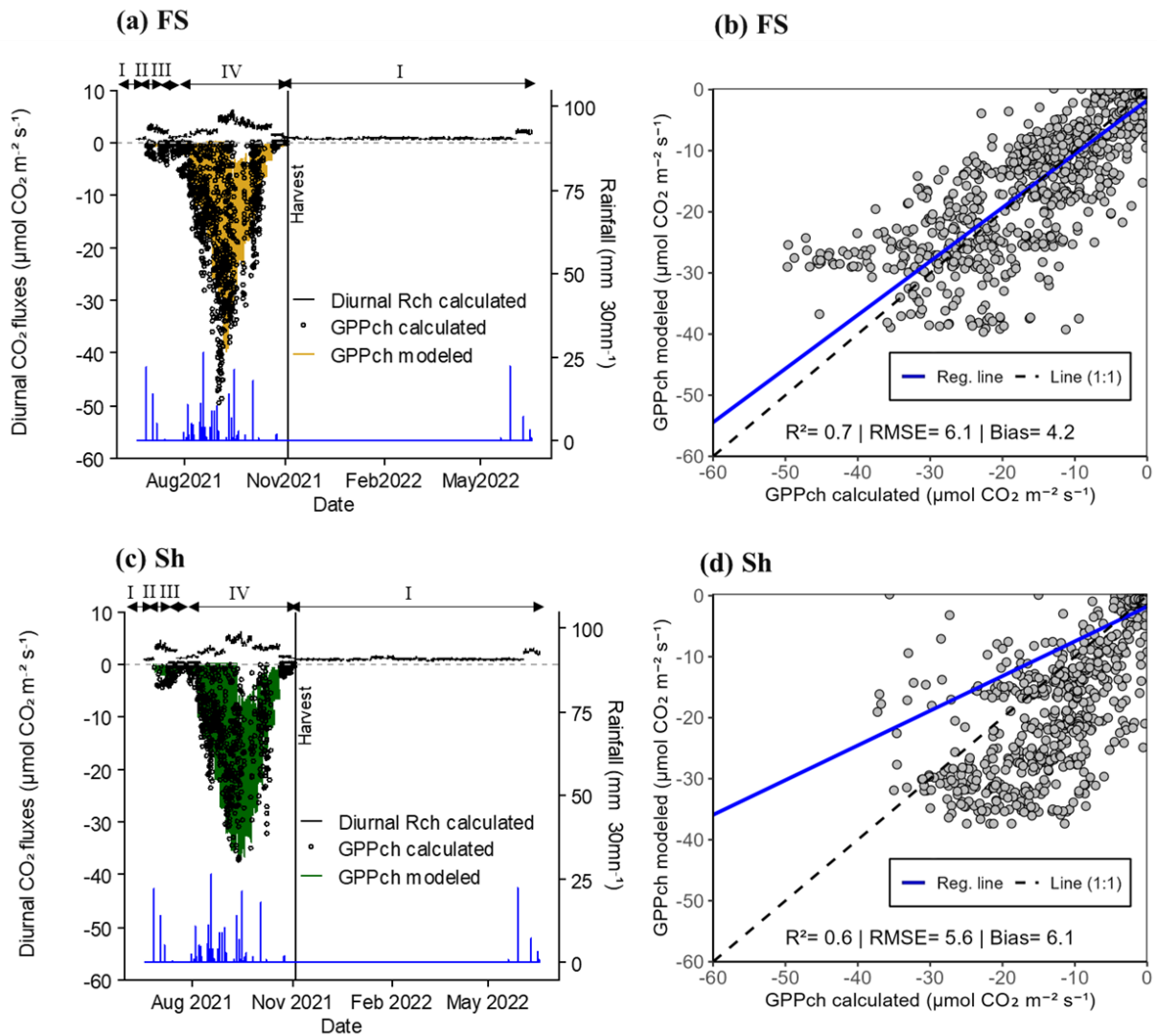
407 (a) and (c): measured nocturnal respiration in chambers (Rch: black dots; average of measurements in 4
 408 chambers per location) vs. modeled (coloured line). The vertical black line indicates the harvest date of
 409 groundnuts inside the chambers. The red arrows indicate the 'Birch' effect and the blue line represents the
 410 rainfall (mm 30mn⁻¹). Roman numerals (above the black arrows) refer to vegetation conditions prevailing
 411 inside the chambers, i.e. (I) bare soil, (II) weeds, (III) weeds + groundnuts, and (IV) groundnuts only.
 412 (b) and (d): scatter plot between measured and modeled nocturnal Rch. The solid blue line indicates the
 413 regression line and the dashed black one the (1:1) line RMSE and bias are expressed as fluxes (in μmol CO₂
 414 m⁻² s⁻¹). Each point represents the mean value from 4 chambers within the FS or Sh environments.

415 *3.2.3. Dynamics of daytime fluxes in chambers*

416 The measured GPP_{ch} stand, as well as GPP modeled with Eq. 6, showed similar seasonal dynamics
417 in FS and Sh (Fig. 4, a and c). The fluxes peaked during the rainy season (Fig. 4a and c), coinciding
418 with periods of vigorous vegetative growth characterised by a high leaf area index (LAI_{ch}) of
419 groundnut plants within the chambers (Fig. S3). The maximum calculated and standardised
420 GPP_{ch} values reached $-50 \mu\text{mol CO}_2 \text{ m}^{-2} \text{ s}^{-1}$ for FS and $-37 \mu\text{mol CO}_2 \text{ m}^{-2} \text{ s}^{-1}$ for Sh. As expected,
421 these fluxes were nil during the dry season when the soil was bare (Fig. 4, a and c).

422 The modeled GPP_{ch} values closely followed the same trends as the calculated values, although
423 model performance was slightly better for FS ($R^2 = 0.7$ with bias and RMSE values of 4.2 and 6.1
424 $\mu\text{mol CO}_2 \text{ m}^{-2} \text{ s}^{-1}$, respectively) compared to Sh ($R^2 = 0.6$ with bias and RMSE values of 6.1 and
425 $5.6 \mu\text{mol CO}_2 \text{ m}^{-2} \text{ s}^{-1}$, respectively) (Fig. 4, b and d).

426 The calculated diurnal respiration values (diurnal R_{ch} calculated) for FS and Sh revealed a 'Birch
427 effect' similar to that observed during the night, though slightly more pronounced under Sh by a
428 factor of 1.2. Diurnal R_{ch} values increased significantly during the rainy season, reaching a
429 maximum of $6.0 \mu\text{mol CO}_2 \text{ m}^{-2} \text{ s}^{-1}$ for both FS and Sh (Fig. 4, a and c). In the dry season, on bare
430 soil, these values declined, with maximum respiration reaching only $0.5 \mu\text{mol CO}_2 \text{ m}^{-2} \text{ s}^{-1}$ for both
431 situations (FS and Sh) (Fig. 4, a and c).



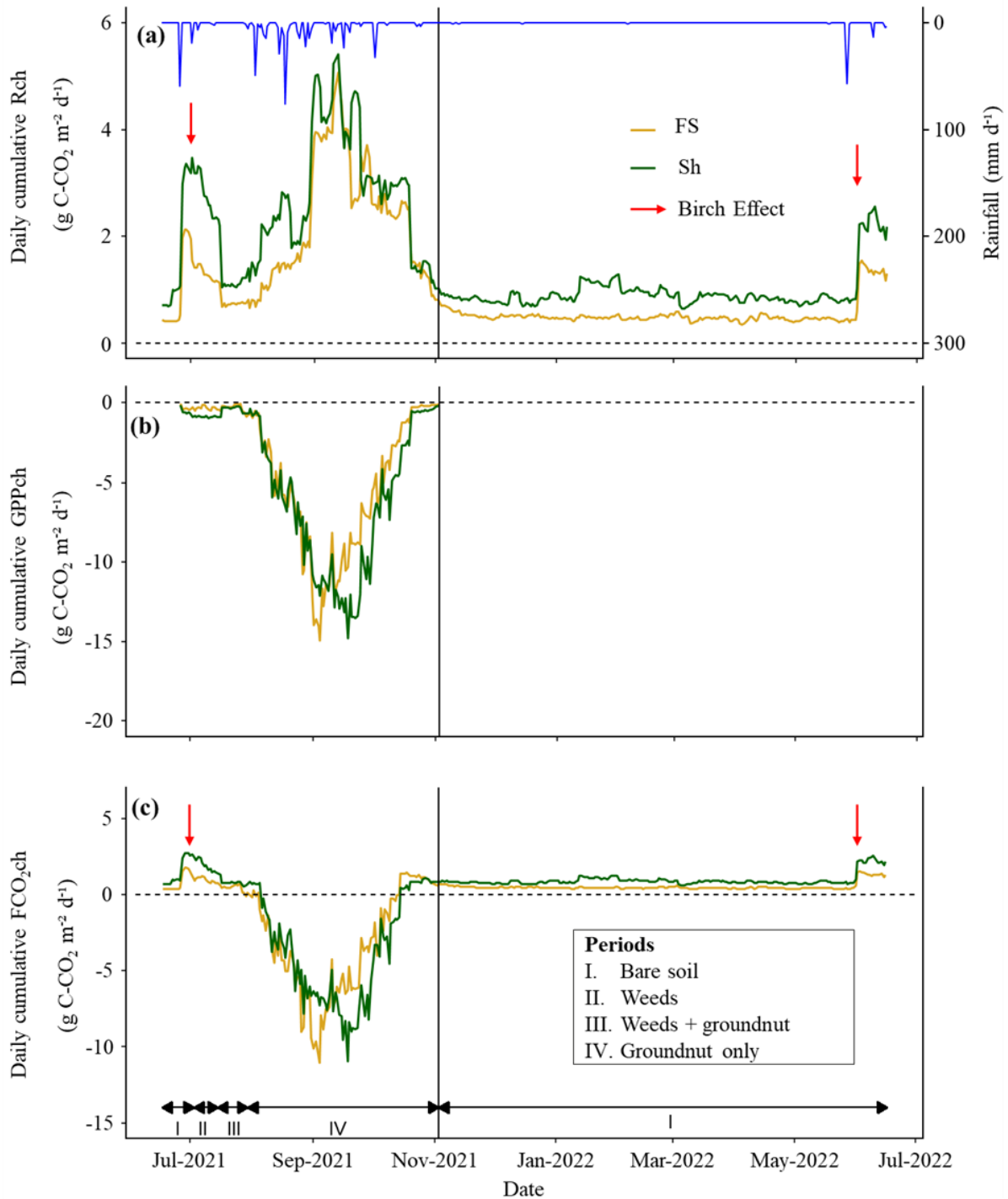
432 Fig. 4: Dynamics of instantaneous diurnal CO₂ fluxes in chambers in Full sun (FS; a and b) and
 433 Shaded (Sh; b and d) environments (filtered based on R² of the CO₂ variation over the time closure
 434 in FS and Sh and Minimum Detectable Flux, Eq.2).

435 (a) and (c): non-gap-filled diurnal Rch calculated (black line, positive values; average of measurements in
 436 4 chambers per location) and GPPch calculated from Eq.5 then standardised for LAI (black dots, negative
 437 values) and modeled (coloured line, negative values). The vertical black line indicates the harvest date of
 438 groundnuts inside the chambers and the blue line represents the rainfall (mm 30mn⁻¹). Roman numerals
 439 (above the black arrows) refer to conditions prevailing inside the chambers, i.e., (I) bare soil, (II) weeds,
 440 (III) weeds + groundnuts, and (IV) groundnuts.

441 (b) and (d): scatter plot between calculated and modeled GPPch. The solid blue line indicates the regression
 442 line and the dashed black one the (1:1) line. RMSE and bias are expressed as fluxes (in μmol CO₂ m⁻² s⁻¹).
 443 Each point represents the mean value from 4 chambers within the FS or Sh environments.

444 *3.3. Dynamics of daily cumulative CO₂ fluxes in chambers*

445 The seasonality of daily cumulative of GPPch stand showed similar dynamics between FS and Sh,
446 with higher variability during the rainy season than during the dry season (Fig. 5). Daily total Rch
447 peaked during the rainy season at 5.1 g C-CO₂ m⁻² d⁻¹ for FS and 5.4 g C-CO₂ m⁻² d⁻¹ for Sh, while
448 the maximum GPPch stand values were comparable at around -15.0 g C-CO₂ m⁻² d⁻¹ for both FS
449 and Sh (Table 1; Fig. S7, a, b, c, and d). In the dry season, Rch decreased (Fig. 5), averaging 0.5 g C-
450 CO₂ m⁻² d⁻¹ for FS and 1.0 g C-CO₂ m⁻² d⁻¹ for Sh. GPPch declined well before harvest (senescence)
451 and remained nil during the dry season (Fig. 5). During the rainy season FCO₂ch peaked in
452 absolute value at around 11.0 g C-CO₂ m⁻² d⁻¹ for FS and Sh (Fig. 5) (Table 1; Fig. S7, e and f),
453 while FCO₂ch values were the same as Rch during the dry season. In absolute terms, the mean Rch
454 and GPPch were significantly higher under Sh as compared to FS, by factors of 1.3 and 1.2,
455 respectively. Conversely, the mean FCO₂ch was significantly higher in absolute value under FS
456 (0.4 g C-CO₂ m⁻² d⁻¹) than under Sh (0.2 g C-CO₂ m⁻² d⁻¹) (Table 1).
457 The annual cumulative Rch values were 392.8 g C-CO₂ m⁻² for FS and 574.5 g C-CO₂ m⁻² for Sh.
458 The GPPch fluxes reached -539.5 g C-CO₂ m⁻² for FS and -632.6 g C-CO₂ m⁻² for Sh. The net annual
459 cumulative C exchange (FCO₂ch) was -146.7 g C-CO₂ m⁻² in FS and -58.1 g C-CO₂ m⁻² in Sh.



460 Fig. 5: Seasonal dynamics of daily gap-filled cumulative fluxes (in gC-CO₂ m⁻² d⁻¹) in chambers.

461 (a) soil+crop respiration (Rch), (b) photosynthesis (GPPch, standardised for LAI) and (c) net CO₂ exchange
 462 (FCO₂ch). The yellow and green solid lines compare the FS and Sh environments, respectively. The vertical
 463 black line indicates the harvest date of groundnuts inside the chambers. The blue line depicts the daily
 464 cumulative rainfall (mm d⁻¹) throughout the rainy season, and the red arrow indicates the 'Birch'
 465 effect. Roman numerals (above the black arrows) in (a) and (c) refer to the prevailing conditions inside the
 466 chambers: (I) bare soil, (II) weeds, (III) weeds + groundnuts, (IV) groundnuts.

467 Table 1: Comparison of daily cumulative and gap-filled chamber CO₂ fluxes (Rch, GPPch
 468 standardised for LAI, and FCO₂ch in g C-CO₂ m⁻²) in the FS and Sh condition.

469

	Annual sum	Daily Mean \pm SD	Min	Max	Mann-Whitney test
(g C-CO ₂ m ⁻²)	.yr ⁻¹	.d ⁻¹	.d ⁻¹	.d ⁻¹	
Rch					
FS	392.8	1.1 \pm 0.9	0.4	5.1	
Sh	574.5	1.6 \pm 1.1	0.6	5.4	*
GPPch					
FS	-539.5	-4.1 \pm 4.3	< -0.1	-14.9	
Sh	-632.6	-4.8 \pm 4.6	< -0.1	-14.8	*
FCO₂ch					
FS	-146.7	-0.4 \pm 2.4	-11.0	1.8	
Sh	-58.1	-0.2 \pm 2.7	-10.9	2.8	*

470 Annual sum corresponds to the annual cumulative fluxes (g C-CO₂ m⁻² yr⁻¹). Mean, SD, Min, and Max
 471 represent respectively the mean, standard deviation, minimum, and maximum values at the daily scale (g
 472 C-CO₂ m⁻² d⁻¹). Asterisks (*) indicate the p-values from the Mann-Whitney test, used to assess differences in
 473 mean between FS and Sh (p < 0.05). Positive values indicate CO₂ emissions, while negative values represent
 474 CO₂ uptake.

475 *3.4. Drivers of daily respiration and photosynthesis in chambers*

476 The chamber-based daily cumulative respiration (Rch) and GPPch showed significant and positive
477 correlations with the leaf area index (LAIch), both at a distance from the trees (FS) and under the
478 trees (Sh) (Table 2). The influence of LAIch on GPPch was stronger ($r = 0.86$ for FS and Sh) than
479 its influence on Rch ($r = 0.60$ for FS; $r = 0.69$ for Sh). Soil VWC was also positively correlated with
480 Rch and GPPch, both in FS and Sh. However, the influence of soil VWC on Rch was stronger under
481 Sh compared to FS, while its influence on GPPch was similar in both situations (FS and Sh). Soil
482 temperature showed weak negative correlations with Rch (in FS and Sh) and with GPPch (only in
483 Sh). Finally, no significant correlations were found between T_{air} , and any of the CO₂ fluxes (Table
484 2).

485 Table 2: Spearman correlation matrix based on daily cumulative and gap-filled CO₂ fluxes from full
 486 year chamber measurements (g C-CO₂ m⁻² d⁻¹) with microclimatic parameters.

Parameters	Condition	r-coef. (Rch)	p (Rch)	r-coef. (GPPch)	p (GPPch)
T _{soil}	FS	-0.25 ***	7.47 x 10 ⁻⁴	ns	1.18 x 10 ⁻³
	Sh	-0.28 ***	9.69 x 10 ⁻¹⁴	-0.38 ***	2.88 x 10 ⁻⁷
T _{air}	FS	ns	0.22	ns	0.35
	Sh	ns	0.98	ns	0.15
VWC	FS	0.51 ***	3.00 x 10 ⁻³⁴	0.75 **	6.73 x 10 ⁻³
	Sh	0.78 ***	1.29 x 10 ⁻⁶⁶	0.75*	0.02
LAIch	FS	0.60 ***	1.11 x 10 ⁻⁶¹	0.86 ***	2.23 x 10 ⁻⁸
	Sh	0.69 ***	6.08 x 10 ⁻⁶⁹	0.86 ***	2.11 x 10 ⁻¹²

487 Spearman correlation coefficients (r-coef.) between daily cumulative and gap-filled CO₂ flux components
 488 (Rch and GPPch, with GPPch in absolute terms) and daily mean microclimatic parameters in full sun (FS)
 489 and shaded chambers (Sh). T_{soil} (°C) is the daily mean soil temperature at 6 cm depth, T_{air} (°C) the daily
 490 mean air temperature at 15 cm height, VWC (%) the daily mean volumetric water content (VWC, %), and
 491 LAIch (m⁻² leaf m⁻² soil) the chamber leaf area index value for a given day. Letter p represents the p-value
 492 and significance levels are indicated by (***) p<0.001; ** p<0.01; * p<0.05); ns p > 0.05.

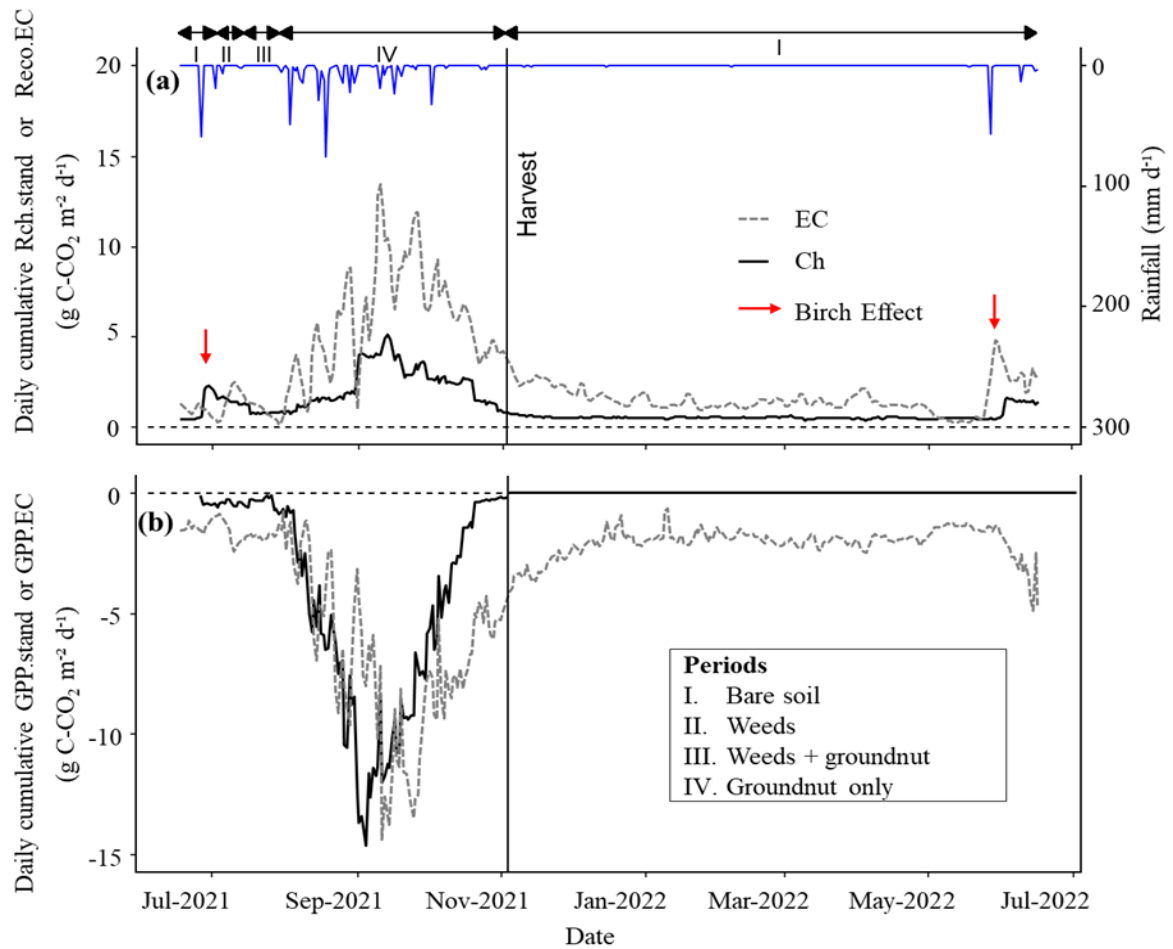
493 3.5. Comparison of respiration and GPP measurements between chambers (Ch) and Eddy
494 Covariance (EC) methods

495 The chamber-based daily total CO₂ fluxes, gap-filled and weighted according tree cover were
496 compared with the fluxes obtained using the EC method (Fig. 6).

497 During the rainy season, both total respiration and GPP showed comparable dynamics between
498 the two methods, with synchronised peaks and higher variability compared to the dry season (Fig.
499 6). The maximum value of Reco.EC, peaked at 13.5 g C-CO₂ m⁻² d⁻¹ (Table 3). The initial value of
500 Rch.stand was comparable to Reco.EC but peaked only at 5.1 g C-CO₂ m⁻² d⁻¹ (Table 3), meaning
501 a third of the peak of Reco.EC. The maximum GPP, was -14.3 g C-CO₂ m⁻² d⁻¹ and -14.6 g C-CO₂
502 m⁻² d⁻¹ for GPP.EC and GPPch.stand, respectively (Table 3). This indicates that the LAI-based
503 standardisation and upscaling approach were realistic, at least up to the peak of groundnut
504 growth.

505 On average, Reco.EC was significantly higher than Rch.stand, by a factor of 2.3. GPP.EC was also
506 significantly higher than GPPch.stand, but only by a factor of 1.2 (Table 3).

507 During the dry season, Reco.EC and Rch.stand gradually decreased. The values for Reco.EC
508 remained higher than for Rch.stand, which was fairly consistent with the contribution of the Ra
509 tree above-ground compartment, even if this difference seemed to disappear at the end of the dry
510 season (Fig. 6). The measured 'Birch effect' was highest for Rch.stand in 2021, but was the
511 opposite in 2022 due to a system failure at the beginning of the rainy season. The maximum value
512 of GPP.EC reached -2.4 g C-CO₂ m⁻² d⁻¹ when the trees were at their maximum of foliage, after
513 harvest and while weeds were still present in the field. However, after the harvest, chamber
514 photosynthesis (GPPch.stand) was nil (Table 3).



515 Fig 6: Comparing the seasonal dynamics of CO₂ fluxes between Eddy Covariance (EC)
 516 measurements and upscaled chamber measurements (ch.stand).

517 (a) represent the seasonal dynamics of soil + crop respiration (Rch.stand) and ecosystem respiration
 518 (Reco.EC) and (b) photosynthesis (GPP.stand and GPP.EC). The black and dashed grey lines show Ch and
 519 EC seasonal dynamics, respectively. The vertical black line indicates the harvest date of groundnuts inside
 520 the chambers. The blue line depicts the daily cumulative rainfall (mm d⁻¹), and the red arrow indicates the
 521 'Birch' effect. Roman numerals (above the black arrows) refer to conditions prevailing inside the
 522 chambers: (I) bare soil, (II) weeds, (III) weeds + groundnuts, (IV) groundnuts.

523 Table 3: Comparison of gap-filled CO₂ fluxes between Eddy Covariance (EC) and upscaled chamber (Ch.stand) measurements, by season (rainy or dry).

	Rainy season				Dry season			
	Daily Mean ± SD (g C-CO ₂ m ⁻²) .d ⁻¹	Min .d ⁻¹	Max .d ⁻¹	Mann-Whitney test	Daily Mean ± SD (g C-CO ₂ m ⁻²) .d ⁻¹	Min .d ⁻¹	Max .d ⁻¹	Mann-Whitney test
Reco.EC or Rch.stand								
EC	4.6 ± 3.2	0.2	13.5	*	1.2 ± 0.4	0.3	2.1	*
Ch.stand	2.0 ± 1.1	0.5	5.1		0.5 ± 0.04	0.4	0.6	
GPP.EC or GPPch.stand								
EC	-5.1 ± 3.6	-0.7	-14.3	*	-1.7 ± 0.3	-0.6	-2.4	
Ch.stand	-4.2 ± 4.3	<-0.1	-14.6		0	0	0	-

524 Mean, SD, Min, and Max represent the daily mean fluxes, standard deviation, minimum, and maximum values, respectively (g C- CO₂ m⁻² d⁻¹). The Asterisks (*) indicate
525 the p-values from the Mann-Whitney test, used to assess differences in mean between EC and Ch. Positive values indicate CO₂ emissions, while negative values
526 represent CO₂ uptake.

527 *3.6. The contribution of F. albida to Reco and GPP*

528 During the dry season, the cumulative contribution of *F. albida* to ecosystem respiration (Ra tree)
529 was 139.6 g C-CO₂ m⁻². This represent 14% of the total annual cumulative Reco, which was
530 estimated at 1000.0 g C-CO₂ m⁻² (Table S4). The contribution of trees (GPP tree) to total annual
531 GPP in absolute term was 270.2 g C-CO₂ m⁻², equivalent to ~23% of the total annual cumulative
532 GPP of the ecosystem measured by EC (1180.0 g C-CO₂ m⁻²) (Table S4).
533 The ratio between these two components (Ra tree / GPP tree) in absolute terms was 0.52,
534 reflecting a carbon use efficiency (CUE) of 0.48 (Table S4).

535 *3.7. Annual vertical CO₂ balances at the field-scale*

536 The upscaled chamber-based annual cumulative total respiration flux (Rch.stand) was estimated
537 to be 4.1 ± 0.18 Mg C-CO₂ ha⁻¹ (Table 4). In comparison, the annual Reco.EC was 10.0 ± 0.49 Mg
538 C-CO₂ ha⁻¹ (Table 4), more than two times larger than Rch.stand.
539 The upscaled GPPch.stand reached an annual cumulative value of -5.5 ± 0.83 Mg C-CO₂ ha⁻¹,
540 whereas the annual cumulative GPP.EC was -11.8 ± 0.53 Mg C-CO₂ ha⁻¹ (Table 4).
541 The net annual vertical C balance, based on both methods, was estimated at -1.4 ± 0.46 Mg C-CO₂
542 ha⁻¹ for chambers (FCO₂ch.stand) and -1.8 ± 0.17 Mg C-CO₂ ha⁻¹ for Eddy Covariance (NEE.EC)
543 (Table 4).

544 Table 4: Annual budget of CO₂ fluxes based on Eddy Covariance (EC) and upscaled chamber
 545 methods (Ch.stand).

	Annual sum (Mg C-CO ₂ ha ⁻¹)	Std error (Mg C-CO ₂ ha ⁻¹)
Reco.EC or Rch.stand		
EC	10.0	0.49
Ch.stand	4.1	0.18
GPP.EC or GPPch.stand		
EC	-11.8	0.53
Ch.stand	-5.5	0.83
NEE.EC or FCO₂ch.stand		
EC	-1.8	0.17
Ch.stand	-1.4	0.46

546 Annual sum corresponds to the annual cumulative fluxes for full year measurements (Mg C-CO₂ ha⁻¹). EC
 547 refers to fluxes measured by the Eddy Covariance method, and Ch refers to the fluxes measured by
 548 chambers, which are then upscaled to the whole field. Rch.stand represents the chamber respiration, while
 549 Reco.EC denotes the ecosystem respiration according to the EC method. GPP.EC and GPPch.stand are the
 550 gross primary production or photosynthesis flux, measured by EC and Ch methods, respectively. NEE.EC
 551 and FCO₂ch.stand represent the net ecosystem exchange for EC and Ch, respectively. The associated
 552 standard error is denoted as Std error (Mg C-CO₂ ha⁻¹). Positive values indicate CO₂ emissions, while
 553 negative values represent CO₂ uptake.

554 4. Discussion

555 4.1. Soil respiration modeling and limitations

556 In this study the Lloyd and Taylor (1994) model, based on a modified Arrhenius-type formulation,
557 was used to model nocturnal soil respiration fluxes for estimating daytime respiration. Unlike the
558 classical Arrhenius equation, this model includes the $(T_{\text{soil}} - T_0)$ term in the denominator of the
559 exponential expression (Eq. 4), which inherently limits the effects of high temperatures by
560 progressively reducing the temperature sensitivity of soil respiration as temperatures rise above
561 a given threshold. This structural feature produces a flattening of the respiration-temperature
562 relationship at elevated temperatures, thereby preventing the overestimations (Lloyd and Taylor,
563 1994).

564 The Lloyd and Taylor model has successfully been widely applied, primarily in boreal and
565 temperate ecosystems (Lasslop et al., 2010; Reichstein et al., 2003), and relies on the assumption
566 of comparable thermal conditions between daytime and nighttime periods (Juszczak et al., 2012).
567 In our study, instantaneous soil temperatures ranged from 20.7 to 45.8 °C during the day and from
568 22.1 to 45.0 °C at night, indicating largely overlapping thermal ranges between the two periods.
569 Model parameters were recalibrated using five-day fixed windows, which provided sufficient
570 temporal resolution while capturing seasonal dynamics of soil respiration.

571 This study represents one of the first applications of the Lloyd and Taylor model in a Sahelian
572 semi-arid context. While Arrhenius based models are known to potentially overestimate fluxes
573 under extreme temperatures due to physiological limitations, over the range of temperatures
574 observed in this study, the modeled soil respiration was not overestimated (Fig. S6, a and b). Thus,
575 the model used in this study appears to provide a realistic representation of soil respiration under
576 local conditions. However, this conclusion is site-specific and should not be interpreted as a
577 general validation of temperature-based models across all semi-arid environments. Such models
578 should be systematically validated with respect to temperature to ensure their reliability.

579 4.2. Seasonality and drivers of chamber-based CO₂ fluxes

580 In our agroforestry context, seasonal variability in CO₂ fluxes closely followed rainfall dynamics,
581 peaking during the wet season and declining sharply in the dry season, consistent with soil
582 moisture depletion and crop senescence. This pattern is typical of semi-arid ecosystems (Ago et
583 al., 2016a; Brümmer et al., 2008; Guillen-Cruz et al., 2023; Macharia et al., 2020; Mosongo et al.,
584 2022; Wieckowski et al., 2024).

585 Respiration and photosynthesis were primarily driven by soil moisture and LAI, reflecting the
586 system's sensitivity to water availability and crop dynamics. Soil moisture enhanced both
587 processes by stimulating microbial activity and supporting plant growth (Borken et al., 2002;

588 Conant et al., 2004; Merbold et al., 2009; Yu et al., 2020; Zhao et al., 2016). The stronger correlation
589 between soil moisture and respiration under *F. albida* canopy (Sh: $r = 0.78$) compared to full sun
590 (FS: $r = 0.51$) suggests greater microbial sensitivity to moisture beneath trees. This likely reflects
591 enhanced substrate availability, resulting in stronger post-rainfall respiration pulses (Meisner et
592 al., 2015) and supporting the 'fertile island' effect, where trees improve local soil conditions
593 (Eldridge et al., 2024). Photosynthetic capacity also responded to soil moisture, as shown by
594 positive correlations with LAI and key physiological traits such as light use efficiency (α) and
595 maximum CO_2 uptake rate (β) (Gonsamo et al., 2019; Qiu et al., 2023; Zhang et al., 2024).
596 In contrast, the influence of soil temperature (T_{soil}) on respiration was weakly negative in both FS
597 and Sh, indicating a thermal threshold beyond which respiration declined —estimated at 32 ± 1.5
598 $^{\circ}\text{C}$ in FS and 29.5 ± 1.9 $^{\circ}\text{C}$ in Sh (Fig. S9, a and b), similar to findings in Eastern Ghana (Owusu et
599 al., 2024). This inhibition likely results from decreased enzymatic and microbial activity under
600 combined heat and water stress (Liu et al., 2018; Richardson et al., 2012). In semi-arid regions,
601 soil respiration often becomes decoupled from temperature due to seasonal moisture constraints
602 (Jia et al., 2020; Tucker & Reed, 2016; Warren, 2014), with microbial activity limited during dry
603 periods despite favourable temperatures. This decoupling helps explain the weak or absent
604 correlation between T_{soil} and soil moisture (Fig. S8, b), particularly under Sh ($r = -0.28$).
605 Management practices such as organic inputs can also modulate these dynamics, adding further
606 variability to soil respiration responses (Meena et al., 2020; Oyonarte et al., 2012; Rong et al.,
607 2015; Xue & Tang, 2018).

608 4.3. Magnitude of chamber-based total CO_2 respiration fluxes

609 Mean total soil respiration values were consistent with those reported in other low-input
610 agricultural systems across sub-Saharan Africa (Mapanda et al., 2010; Pelster et al., 2017;
611 Rosenstock et al., 2016). In full sun (FS), the mean respiration (1.0 ± 0.9 $\text{g C-CO}_2 \text{ m}^{-2} \text{ d}^{-1}$) closely
612 matched values measured by Wachiye et al. (2020) in a semi-arid Kenyan field at 1158 m altitude
613 (1.1 ± 0.1 $\text{g C-CO}_2 \text{ m}^{-2} \text{ d}^{-1}$). This similarity likely reflects comparable environmental conditions,
614 including moderate rainfall (~ 550 mm yr^{-1}) and low soil organic carbon and nitrogen contents
615 ($<1\%$) in the 0–20 cm layer of sandy soil. In contrast, respiration under *F. albida* canopy (Sh: 1.6
616 ± 1.1 $\text{g C-CO}_2 \text{ m}^{-2} \text{ d}^{-1}$) was higher, likely due to additional autotrophic respiration from tree roots
617 and greater organic inputs beneath the canopy. Nonetheless, this flux remains close to values
618 observed in low-input sorghum fields on sandy loam soils in eastern Ghana (1.7 ± 1.1 $\text{g C-CO}_2 \text{ m}^{-2}$
619 d^{-1}), despite higher rainfall (950–1000 mm yr^{-1}) in that region (Owusu et al., 2024).
620 Cumulative annual respiration fluxes fell within the range reported for Sahelian croplands (250–
621 450 $\text{g C-CO}_2 \text{ m}^{-2}$) (Brümmer et al., 2009) and other sub-Saharan African agricultural systems (Kim
622 et al., 2016). The cumulative flux under tree cover is similar to that measured in cassava fields in

623 eastern Tanzania ($440 \text{ g C-CO}_2 \text{ m}^{-2} \text{ yr}^{-1}$), despite the latter receiving higher rainfall ($\sim 1115 \text{ mm}$
624 yr^{-1}) (Rosenstock et al., 2016). This convergence may stem from comparable soil fertility
625 constraints, with low soil organic carbon (1–1.7%) and nitrogen contents ($<0.5\%$). In contrast,
626 the slightly lower cumulative flux in FS may reflect less favourable microclimatic conditions—
627 such as elevated soil temperatures and increased aridity away from tree cover—limiting
628 microbial activity (see Section 4.1).

629 Across sub-Saharan Africa, soil respiration fluxes based on static chamber measurements show
630 high spatial variability, largely shaped by climate and land use. For example, Owusu et al. (2024)
631 found higher respiration in woodlands ($3.8 \pm 0.8 \text{ g C-CO}_2 \text{ m}^{-2} \text{ d}^{-1}$) and grazed areas (2.7 ± 1.7)
632 than in croplands (1.7 ± 1.1) in humid eastern Ghana. This gradient was linked to differences in
633 soil moisture and organic matter. Similarly, Rosenstock et al. (2016) reported much higher fluxes
634 in highland pastures in Kenya ($3.8\text{--}4.4 \text{ g C-CO}_2 \text{ m}^{-2} \text{ d}^{-1}$) compared to cultivated fields in eastern
635 Tanzania (1.2 ± 0.2), highlighting the role of vegetation cover and soil fertility.

636 4.4. *Effect of trees on chamber-based soil respiration and photosynthesis*

637 A notable increase in respiration and photosynthesis fluxes was observed under *F. albida* trees
638 (Sh) compared at a distance from trees (FS). This increase may indicate the potential role of *F.*
639 *albida* in modulating CO_2 exchange dynamics (Rch and GPPch) within this agro-silvo-pastoral
640 system. These results are consistent with preliminary findings from similar environments
641 (Duthoit et al., 2020).

642 Numerous studies have investigated the effect of tree species on greenhouse gas fluxes,
643 particularly CO_2 , revealing significant variations across different ecological contexts (Bréchet et
644 al., 2021, 2025; Klaus et al., 2024; Mazza et al., 2021; Ramesh et al., 2013; Rheault et al., 2024).
645 However, the underlying mechanisms by which trees influence these dynamics are not yet fully
646 understood.

647 In general, agroforestry systems have been well-documented for their ability to provide a range
648 of ecosystem services (e.g., Assefa et al., 2024; Bado et al., 2021; Kuyah et al., 2019; Rolo et al.,
649 2023). Specifically, *Faidherbia*-based agroforestry systems may play a crucial role in regulating
650 CO_2 exchanges between the soil and atmosphere. *F. albida*-based agroforestry systems are
651 recognized for enhancing both soil organic and mineral fertility (Bayala et al., 2020; Dilla et al.,
652 2019; Sileshi, 2016; Sileshi et al., 2020; Stephen et al., 2020), mainly through litter accumulation
653 and direct inputs from livestock excreta under their canopies. Additionally, the extensive roots
654 system of *F. albida* trees helps concentrate mineral nutrients, contributing to the formation of a
655 'fertile island' effect under the trees (Siegwart et al., 2022; Eldridge et al., 2024). Moreover, *F.*
656 *albida* improve water infiltration (Diongue et al., 2023; Faye et al., 2020; Sarr et al., 2023), enhance
657 soil moisture retention (Clermont-Dauphin et al., 2023) and contribute to reduced soil

658 temperatures (de Carvalho et al., 2021; Lopes et al., 2024; Sida et al., 2018). These changes foster
659 a more favourable environment for soil microbial activity and crop development (Diack et al.,
660 2024; Diene et al., 2024; Leroux et al., 2020; Roupsard et al., 2020) under the trees compared to
661 open areas. Consequently, this likely explains the stronger effect of soil moisture and the leaf area
662 index of groundnuts on Rch under the trees, resulting in higher total respiration (Table 2). For
663 photosynthesis, the effect of these parameters was similar in both FS and Sh (Table 2). However,
664 the significantly higher intensity of GPPch under Sh can be explained by greater light use efficiency
665 (α) and a higher maximum CO₂ uptake rate at light saturation (β) in this shaded environment. In
666 agroforestry systems, light use efficiency can at least partially mitigate the reduction in
667 photosynthetically active radiation under tree canopies (Charbonnier et al., 2017).
668 Similar results have been observed in different climatic conditions and ecosystems. Gomes et al.
669 (2016) investigated soil respiration using mobile chambers (LI-8100-102 model) under trees in
670 coffee-based agroforestry systems and in the open areas in Minas Gerais, Brazil. These studies
671 were conducted with agroecological management practices, such as weeding, intercropping maize
672 between coffee rows, and mulching. The agroforestry systems exhibited lower air and soil
673 temperatures (at 5 and 10 cm depth) and higher air and soil humidity compared to the open areas
674 (Gomes et al., 2016). These authors observed greater spatial variability in soil respiration in
675 agroforestry system (34.1%) compared to the open areas (24.2%). This variability was mainly
676 linked with fluctuations in labile carbon and total nitrogen, reflecting more favourable soil
677 microclimate for microbial activity in agroforestry system. In contrast, soil temperature (10 cm
678 depth) accounted for most of the variability observed in the open areas, where the absence of tree
679 canopy resulted in high soil temperatures and low soil moisture (Gomes et al., 2016). Likewise,
680 Haren et al. (2010) reported 38% higher soil respiration near large trees (DBH > 35 cm) in clay-
681 rich Amazonian forests compared to open sites. Interestingly, the magnitude of CO₂ fluxes was
682 independent of tree species, indicating that canopy effects may outweigh species-specific traits in
683 some contexts. In our study, *F. albida*'s influence on CO₂ fluxes aligns with this general pattern
684 observed in tropical agroforestry. However, the mechanisms linking individual tree species to
685 microbial and physicochemical drivers of CO₂ dynamics remain insufficiently understood and
686 warrant further investigation (Jevon et al., 2023).

687 4.5. Birch Effect

688 A rapid increase in soil respiration was observed following the first rainfall events, particularly
689 under *F. albida*. This phenomenon can be attributed to the lower bulk density of the soil under the
690 trees (Clermont-Dauphin et al., 2023; Siegwart et al., 2023), which potentially lead to CO₂
691 accumulation during the dry season due to higher soil organic matter (SOM) (Siegwart et al.,
692 2023). Additionally, the sensitivity of microbial communities to subtle variations in soil moisture,

693 compounded by the tree effect, may further explain this phenomenon, as outlined in Sections 4.1
694 and 4.3. This phenomenon, known as the 'Birch effect' (Birch, 1958), has been reported across
695 various semi-arid ecosystems in sub-Saharan Africa (Ago et al., 2016b; Fan et al., 2015;
696 Wieckowski et al., 2024), as well as other semi-arid ecosystems globally (Roby et al., 2022; Yan et
697 al., 2014; Yu et al., 2020). In these contexts, the 'Birch effect' may result from the displacement of
698 soil gas phases by the piston effect generated during water infiltration (Singh et al., 2023).
699 Furthermore, microbial communities in semi-arid environments adopt osmoregulatory
700 mechanisms to withstand water deficit (Warren, 2014), which is particularly pronounced during
701 the dry season. This phenomenon reduces soil microbial metabolism (Schimel et al., 2007). Upon
702 rapid soil rewetting, especially after prolonged dry periods, soil microbial metabolism process is
703 swiftly reactivated, leading to a transient pulse in respiration and a CO₂ release (Barnard et al.,
704 2020; Kim et al., 2012; Manzoni et al., 2020; Vargas et al., 2018). Isotopic signatures of soil
705 respiration provide evidence supporting the hypothesis that these pulses result from the rapid
706 mineralisation of necromass or osmolytes excreted by microorganisms under drought stress
707 (Schimel et al., 2007; Unger et al., 2010). Additional factors may amplify the 'Birch effect'. For
708 instance, drying-rewetting cycles can induce physical disruption of soil aggregates, enhance
709 oxygen penetration and thereby expose previously protected organic matter to microbial
710 decomposition (Rabbi et al., 2024). This increases substrate availability and subsequently boosts
711 soil respiration fluxes.

712 The magnitude of the 'Birch effect' is modulated by the severity and duration of drought. Thus, at
713 our study site, given the 8- to 9-month-long dry season, the 'Birch effect' is particularly intense.
714 Indeed, extended drought periods promote greater accumulation of microbial necromass and
715 intensify hypo-osmotic stress responses upon rewetting (Singh et al., 2023).

716 *4.6. Comparing EC and chamber-based methods*

717 Results revealed high seasonal variability, with higher values during the rainy season compared
718 to the dry season. This seasonal pattern aligns with findings from studies in the Sahel using the
719 EC method for CO₂ flux measurements (Brümmer et al., 2008; Tagesson et al., 2015; Agbohessou
720 et al., 2023, Wieckowski et al., 2024). Comparable patterns have also been documented at the
721 ecosystem scale in other semi-arid environments (Ago et al., 2014; Archibald et al., 2009; Ardö et
722 al., 2008; Jia et al., 2020; Quansah et al., 2015; Williams et al., 2009; Zhang, Bi, et al., 2024).

723 Several comparative studies between chamber and EC methods have reported both congruent
724 and divergent CO₂ flux estimates (Bastviken et al., 2022; Poyda et al., 2017; Riederer et al., 2014;
725 J. Tang et al., 2008; Wang et al., 2010). In the present study, ecosystem respiration fluxes during
726 the rainy season exhibited notable discrepancies measurements between EC (Reco.EC) and
727 upscaled chamber-based (Rch.stand). This is attributable to differences in the flux components

728 captured by each method. Specifically, Reco.EC included respiration from below- and above-
729 ground tree parts, crops (groundnuts and cowpeas), weeds, and soil, whereas Rch.stand
730 accounted only respiration from below-ground tree, groundnut crop, and soil. Therefore, as
731 expected, Reco.EC (4.6 ± 3.2 g C-CO₂ m⁻² d⁻¹) were significantly higher than Rch.stand (2.0 ± 1.1 g
732 C-CO₂ m⁻² d⁻¹).

733 For chamber-based GPP measurements, values were standardised (GPP-stand) by the field leaf
734 area index (LAI.field). This allowed it to improve comparability with GPP.EC when trees were
735 leafless in the rainy season. In both cases, GPP accounted only for crops (groundnut and cowpea)
736 and weeds, as trees were non-photosynthetic in the rainy season. Despite this standardisation,
737 GPP.EC values (-5.1 ± 3.6 g C-CO₂ m⁻² d⁻¹) were significantly higher than GPPch.stand values (-4.2
738 ± 4.3 g C-CO₂ m⁻² d⁻¹). However, no divergence was observed in August, and the intensity of the
739 peak of GPP in September was similar in both methods, but from the onset of groundnut
740 senescence, when weeds became the dominant photosynthetic contributors. Thus, during the
741 groundnut growth season, with leafless *F. albida* trees and almost no weeds, GPP measurements
742 from EC and chambers generate closely comparable results. Therefore, this provides an initial
743 form of cross-validation between the two methods. It is important to note that the EC method
744 integrates CO₂ fluxes over a larger spatial scale, encompassing all ecosystem components
745 (Baldocchi, 2003), while the chamber method captures fluxes on a smaller scale (i.e., at the 0.25
746 m² scale). This scale disparity can introduce uncertainties when upscaling chamber-based fluxes
747 to the field, as vegetation composition within chambers does not represent the EC footprint
748 average vegetation. This makes upscaling chamber-based measurements challenging.
749 Nevertheless, the standardisation we applied on chamber photosynthesis by LAI has been
750 relatively successful.

751 During the dry season, Reco.EC included respiration from below- and above-ground tree parts
752 (with leaves) and bare soil, while Rch.stand measured only below-ground tree and bare soil
753 respiration. Consequently, the difference between Reco.EC and Rch.stand was solely attributable
754 to above-ground tree respiration (Ra tree above-ground). In terms of GPP, chamber
755 measurements were nil, whereas GPP.EC reflected only GPP trees.

756 The transition period, characterised by groundnut senescence, tree leaf regrowth, and weed
757 proliferation, introduced further complexity, amplifying method-specific discrepancies. Rch.stand
758 measurements facilitated the estimation of tree contribution to Reco.EC (Ra tree) and the
759 verification of the consistency for EC results in terms of carbon use efficiency (CUE), estimated
760 here at 0.48. This value indicates that nearly 50% of the carbon captured by trees is allocated to
761 biomass. The CUE estimate here is well comparable to the global average across diverse
762 ecosystems, climates, and management practices (0.49 ± 0.14) (Tang et al., 2019). Similar CUE
763 values have been reported for semi-arid grasslands (0.46 ± 0.10), but our value is notably lower

764 than those documented for wetlands (0.61 ± 0.13) (Tang et al., 2019). Overall, these findings
765 reinforce the plausibility of our assumptions regarding the compartment contributions to Reco.EC
766 and Rch.stand, thereby providing a second cross-validation of the EC-Ch comparison. However,
767 despite a frequently assumed CUE of 0.5 in models, global estimates span a broad range (0.20 to
768 0.82), depending on ecosystem type and management practices (DeLucia et al., 2007; Tang et al.,
769 2019). This underscores the importance of refining carbon flux models to better represent the
770 biophysical processes governing CO₂ exchange in semi-arid agroforestry systems. The combined
771 use of EC and chamber methodologies offers a comprehensive perspective on ecosystem-scale CO₂
772 flux dynamics, advancing the understanding of carbon cycling in these environments.

773 4.7. *Net annual vertical carbon balance*

774 The net annual carbon balance was quantified at -1.4 ± 0.46 Mg C-CO₂ ha⁻¹ with the chamber
775 method and -1.8 ± 0.17 Mg C-CO₂ ha⁻¹ by the Eddy Covariance (EC), indicating that the studied
776 agro-silvo-pastoral system functions as a net carbon sink. These findings corroborate the system
777 potential role in mitigating greenhouse gas emissions, consistent with previous studies reporting
778 vertical CO₂ flux balances in semi-arid ecosystems (Rahimi et al., 2021; Tagesson et al., 2015;
779 Agbohessou et al., 2023, Wieckowski et al., 2024).

780 The estimated net C exchange balance is close to the reported mean for Sahelian ecosystems (-1.6
781 ± 0.5 Mg C-CO₂ ha⁻¹; Tagesson et al., 2016). The EC-based net C exchange balance (-1.8 ± 0.17 Mg
782 C-CO₂ ha⁻¹) is also similar to the value of -1.9 ± 0.4 Mg C-CO₂ ha⁻¹ reported for semi-arid savannas
783 of northeastern Benin, despite higher annual rainfall (1495 mm; Ago et al., 2016b). Furthermore,
784 our EC estimate is close to the average net C exchange reported for West African terrestrial
785 ecosystems (-2.0 ± 1.5 Mg C-CO₂ ha⁻¹; Ago et al., 2016a).

786 However, estimates from Tagesson et al. (2015) (-2.7 ± 0.07 Mg C-CO₂ ha⁻¹) for a semi-arid
787 savannah in Dahra, Senegal, located between the 300 mm and 400 mm isohyets, were
788 comparatively higher. This is potentially attributable to specific characteristics of that specific
789 savannah site, such as herbaceous vegetation cover during the rainy season, the presence of
790 evergreen trees, and land management practices linked to pastoral livestock activities (Tagesson
791 et al., 2016).

792 The net annual C balance estimates presented in this study are, in fact, representing vertical fluxes
793 only, given that they exclude organic matter (OM) imports and, more critically, exports,
794 introducing uncertainties. Notably, the export of crop residues and direct inputs from animal
795 excreta — particularly significant in 'bush fields' during the dry season — were not accounted for.
796 In our case of 'bush field', crop residues are exported to feed livestock, while livestock faeces are
797 collected for use as fuel or manure in 'home fields'. Such practices may lead to a significant soil
798 organic carbon stocks depletion (Malou et al, 2021), potentially diminishing the net C budget (-

799 $1.4 \pm 0.46 \text{ Mg C-CO}_2 \text{ ha}^{-1}$) over time and shifting the system closer to carbon neutrality (Assouma
800 et al., 2019).

801 These results should be contextualized within the broader framework of climate change and semi-
802 arid ecosystem management. Although agro-silvo-pastoral systems can function as apparent
803 annual carbon sinks, they remain highly sensitive to interannual rainfall variability and escalating
804 anthropogenic pressures. Sustainable management practices, particularly regarding C
805 inputs/outputs from the system regarding crop harvest, residues exportation, and cattle free
806 manuring, must be taken into account to confirm the capacity of the system to act as effective a
807 carbon sink.

808 *4.8. Limitations of the study*

809 This study benefited from the inverse phenology of *F. albida*, allowing for direct comparison
810 between chamber-based GPP (GPPch.stand) and ecosystem-level GPP (GPP.EC) during the
811 leafless period of the trees. However, the system spatial heterogeneity —common in
812 agroforestry— posed challenges for accurately partitioning CO₂ fluxes among trees, crops, and
813 soil. A key limitation was the development of weeds during the late rainy season, which
814 complicated the attribution of fluxes, particularly during the transitional period. Additionally,
815 while GPPch was successfully standardised by LAI for upscaling, this was not feasible for
816 respiration. Respiration integrates both autotrophic and heterotrophic components, which
817 respond to different drivers and are not directly linked to LAI, limiting the precision of upscaled
818 Rch.

819 Future improvements should aim to separately quantify respiration sources —tree roots, crops,
820 and microbial (heterotrophic) respiration— and account explicitly for the weed layer, to refine
821 flux partitioning in such complex agroforestry systems.

822 Furthermore, the present study constitutes only an intermediate step delivering a first integrated
823 estimate of the main vertical CO₂ exchanges (photosynthesis, respiration, and net ecosystem
824 exchange) as a base for a forthcoming paper that will present a more comprehensive carbon
825 budget of the ecosystem. Establishing such a carbon budget would require substantial additional
826 data acquisition and poses considerable methodological challenges. In particular, quantifying
827 carbon inputs/outputs associated with free-ranging livestock grazing would be difficult to achieve
828 with acceptable accuracy. It must also be recognised that the system is in a dynamic, non-steady
829 state, characterised by marked inter-annual variability as well as periods of carbon storage and
830 release, which are difficult to constrain empirically except through modeling.

831 **Conclusion**

832 This study demonstrates the successful application of automated static chambers to quantify CO₂
833 fluxes in a Sahelian agroforestry system dominated by *F. albida*. The continuous, high-frequency
834 measurements captured key seasonal dynamics and short-lived events (e.g., Birch effect),
835 providing a more accurate assessment of carbon exchange than traditional intermittent sampling.
836 By integrating crop and soil components and applying dynamic partitioning models, the study
837 quantified both respiration and photosynthesis fluxes at fine temporal resolution. The results
838 revealed a clear 'fertile island' effect under tree canopies, with higher respiration and
839 photosynthetic activity, and highlighted the significant contribution of *F. albida* trees to annual
840 carbon uptake.

841 The consistency between chamber- and eddy covariance-based estimates reinforces the
842 robustness of the methodology. Overall, this work underscores the role of *F. albida*-based
843 agroforestry systems in the dynamic of C exchanges in semi-arid environments, offering valuable
844 insights for carbon accounting and sustainable land management in the Sahel.

845 **Acknowledgments**

846 This research was financially supported by the CaSSECS project (Carbon Sequestration and
847 Greenhouse Gas Emissions in (Agro) Silvopastoral Systems of the CILS-Sahel States
848 (FOOD/2019/410-169), within the framework of the European Union's initiative 'Development
849 of Smart Innovation through Agricultural Research' (DeSIRA-UE-EuropAID). We extend our
850 sincere gratitude to the coordination team of the CaSSECS project, the "Laboratoire Mixte
851 International Intensification Écologique des Sols Cultivés en Afrique de l'Ouest" (LMI IESOL) of
852 the of the French National Institute for Development (IRD) in Dakar (Senegal), as well as to the
853 Faidherbia-Flux platform (<https://lped.info/wikiObsSN/?Faidherbia-Flux>), its partners, and
854 affiliated projects: EU-H2020 [SUSTAIN-SAHEL (Grant N° 861974)]; ANR under the
855 France 2030 program [PEPR FairCarboN-RIFT (reference ANR-22-PEXF-0004)]; EU-
856 HORIZON EUROPE [GALILEO (Grant N° 101181623)]. Our deepest appreciation goes to Ibou
857 Diouf, the observer at our experimental site. Tagesson also acknowledged funding from Formas
858 (Dnr 2021-00644). Lastly, we are deeply grateful to the two reviewers, Riccardo Picone and
859 Jim Boonman, for their insightful and highly constructive comments.

860 **Author contribution: CRediT**

861 **Seydina Mohamad BA:** Conducting in situ experiments, collecting and processing data,
862 writing-original draft, review and editing. **Olivier Roupsard:** Designing experimental
863 apparatus and methodology, writing, review and editing. **Lydie Chapuis-Lardy:** Designing
864 methodology, writing, review and editing. **Yélognissè Agbohessou:** Processing data,
865 review and editing. **Fred Bouvery:** Designing chambers and connection to the instrument,
866 review and editing. **Maxime Duthoit:** Designing experimental set and methodology,
867 review and editing. **Aleksander Wieckowski:** Review and editing. **Mohamed Habibou**
868 **Assouma:** Review and editing. **Espoir Gaglo:** Processing data, review and editing. **Claire**
869 **Delon:** review and editing. **Torbern Tagesson:** Designing methodology, review, and
870 editing. **Bienvenu Sambou:** Review and editing. **Dominique Serça:** Designing methodology,
871 writing, review and editing.

872 **References**

- 873 Agbohessou, Y., Delon, C., Mougin, E., Grippa, M., Tagesson, T., Diedhiou, M., Ba, S., Ngom, D., Vezy,
874 R., Ndiaye, O., Assouma, M. H., Diawara, M., & Rounsard, O.: To what extent are greenhouse-gas
875 emissions offset by trees in a Sahelian silvopastoral system?, *Agr. Forest. Meteorol.*, 343, 109780,
876 <https://doi.org/10.1016/j.agrformet.2023.109780>, 2023.
- 877 Agbohessou, Y., Delon, C., Grippa, M., Mougin, E., Ngom, D., Gaglo, E. K., Ndiaye, O., Salgado, P., and
878 Rounsard, O.: Modelling CO₂ and N₂O emissions from soils in silvopastoral systems of the West
879 African Sahelian band. *Biogeosciences*, 21, 2811–2837, [https://doi.org/10.5194/bg-21-2811-](https://doi.org/10.5194/bg-21-2811-2024)
880 [2024](https://doi.org/10.5194/bg-21-2811-2024), 2024.
- 881 Ago, E., Agbossou, K., Ozer, P., & Aubinet, M.: Mesure des flux de CO₂ et séquestration de carbone
882 dans les écosystèmes terrestres ouest-africains (synthèse bibliographique), *Biotechnologie*,
883 *Biotechnol. Agron. Soc. Environ.*, 20(1), 68-82, <https://doi.org/10.25518/1780-4507.12565>,
884 2016a.
- 885 Ago, E., Agbossou, E. K., Cohard, J. M., Galle, S., & Aubinet, M.: Response of CO₂ fluxes and
886 productivity to water availability in two contrasting ecosystems in northern Benin (West Africa),
887 *Ann. Forest. Sci.*, 73(2), 483-500, <https://doi.org/10.1007/s13595-016-0542-9>, 2016b.
- 888 Ago, E., Agbossou, E. K., Galle, S., Cohard, J. M., Heinesch, B., & Aubinet, M.: Long term observations
889 of carbon dioxide exchange over cultivated savanna under a Sudanian climate in Benin (West
890 Africa), *Agr. Forest. Meteorol.*, 197, 13-25, <https://doi.org/10.1016/j.agrformet.2014.06.005>,
891 2014.
- 892 Archibald, S. A., Kirton, A., van der Merwe, M.R, Scholes, R. J., Williams, C.A, & Hanan, H.: Drivers of
893 inter-annual variability in Net Ecosystem Exchange in a semi-arid savanna ecosystem, South
894 Africa, *Biogeosciences*, 6, 251–266, <https://doi.org/10.5194/bg-6-251-2009>, 2009.
- 895 Ardö, J., Mölder, M., El-Tahir, B. A., & Elkhidir, H. A. M.: Seasonal variation of carbon fluxes in a
896 sparse savanna in semi-arid Sudan, *Carbon Balance and Management*, 3(1), 7,
897 <https://doi.org/10.1186/1750-0680-3-7>, 2008.
- 898 Assefa, A., Muthuri, C. W., Gebrekirstos, A., Hadgu, K., & Fetene, M.: Tree growth and wheat
899 productivity are affected by pollarding *Faidherbia albida* in semi-arid Ethiopia, *Agroforest. Syst.*,
900 98(3), 783-796, <https://doi.org/10.1007/s10457-023-00948-7>, 2024.

901 Assouma, M. H., Hiernaux, P., Lecomte, P., Ickowicz, A., Bernoux, M., & Vayssières, J.: Contrasted
902 seasonal balances in a Sahelian pastoral ecosystem result in a neutral annual carbon balance,
903 *Journal of Arid Environments*, 162, 62-73, <https://doi.org/10.1016/j.jaridenv.2018.11.013>, 2019.

904 Assouma, M. H., Serça, D., Guérin, F., Blanfort, V., Lecomte, P., Touré, I., Ickowicz, A., Manlay, R. J.,
905 Bernoux, M., & Vayssières, J.: Livestock induces strong spatial heterogeneity of soil CO₂, N₂O and
906 CH₄ emissions within a semi-arid sylvo-pastoral landscape in West Africa, *Journal of Arid Land*,
907 9(2), 210-221, <https://doi.org/10.1007/s40333-017-0001-y>, 2017.

908 Bado, B. V., Whitbread, A., & Sanoussi Manzo, M. L.: Improving agricultural productivity using
909 agroforestry systems: Performance of millet, cowpea, and ziziphus-based cropping systems in
910 West Africa Sahel, *Agr. Ecosyst. Environ.*, 305, 107175,
911 <https://doi.org/10.1016/j.agee.2020.107175>, 2021.

912 Bahn, M., Reichstein, M., Davidson, E. A., Grünzweig, J., Jung, M., Carbone, M. S., Epron, D., Misson,
913 L., Nouvellon, Y., Roupsard, O., Savage, K., Trumbore, S. E., Gimeno, C., Curiel Yuste, J., Tang, J.,
914 Vargas, R., & Janssens, I. A.: Soil respiration at mean annual temperature predicts annual total
915 across vegetation types and biomes, *Biogeosciences*, 7(7), 2147-2157,
916 <https://doi.org/10.5194/bg-7-2147-2010>, 2010.

917 Baldocchi, D.: Assessing the eddy covariance technique for evaluating carbon dioxide exchange
918 rates of ecosystems: Past, present and future, *Glob. Change Biol.*, 9, 479-492,
919 <https://doi.org/10.1046/j.1365-2486.2003.00629.x>, 2003.

920 Baldocchi, D.: « Breathing » of the terrestrial biosphere: Lessons learned from a global network of
921 carbon dioxide flux measurement systems, *Aust. J. Bot.*, 56(1), 1,
922 <https://doi.org/10.1071/BT07151>, 2008.

923 Baldocchi, D.: How eddy covariance flux measurements have contributed to our understanding of
924 global change biology, *Glob. Change Biol.*, 26: 242-260, <https://doi.org/10.1111/gcb.14807>,
925 2020.

926 Barnard, R. L., Blazewicz, S. J., & Firestone, M. K.: Rewetting of soil: Revisiting the origin of soil CO₂
927 emissions, *Soil Biology and Biochemistry*, 147, <https://doi.org/10.1016/j.soilbio.2020.107819>,
928 2020.

929 Bastviken, D., Wilk, J., Duc, N. T., Gålfalk, M., Karlson, M., Neset, T.-S., Opach, T., Enrich-Prast, A., &
930 Sundgren, I.: Critical method needs in measuring greenhouse gas fluxes. *Environmental Research*
931 *Letters*, 17(10), 104009, <https://doi.org/10.1088/1748-9326/ac8fa9>, 2022.

932 Bayala, J., Sanou, J., Bazié, H. R., Coe, R., Kalinganire, A., & Sinclair, F. L.: Regenerated trees in
933 farmers' fields increase soil carbon across the Sahel, *Agroforest. Syst.*, 94(2), 401-415,
934 <https://doi.org/10.1007/s10457-019-00403-6>, 2020.

935 Birch, H. F.: The effect of soil drying on humus decomposition and nitrogen availability, *Plant and*
936 *Soil*, 10(1), 9-31, <https://doi.org/10.1007/BF01343734>, 1958.

937 Bombelli A, Henry M., Castaldi S., Adu-Bredu S, Arneth A, De Grandcourt A, Grieco E., Kutsch
938 W.L., Lehsten V., Rasile A., Reichstein M, Tansey K, Weber U, Valentini R.: An outlook on the Sub-
939 Saharan Africa carbon balance, *Biogeosciences*, 6 (10), 2193-2205, [https://doi.org/10.5194/bg-](https://doi.org/10.5194/bg-6-2193-2009)
940 [6-2193-2009](https://doi.org/10.5194/bg-6-2193-2009), 2009.

941 Boroken, W., Xu, Y., Davidson, E. A., & Beese, F.: Site and temporal variation of soil respiration in
942 European beech, Norway spruce, and Scots pine forests, *Glob. Change Biol.*, 8(12), 1205-1216,
943 <https://doi.org/10.1046/j.1365-2486.2002.00547.x>, 2002.

944 Bréchet, L. M., Daniel, W., Stahl, C., Burban, B., Goret, J. Y., Salomón, R. L., & Janssens, I. A.:
945 Simultaneous tree stem and soil greenhouse gas (CO₂, CH₄, N₂O) flux measurements: A novel
946 design for continuous monitoring towards improving flux estimates and temporal resolution, *New*
947 *Phytologist*, 230(6), 2487-2500, <https://doi.org/10.1111/nph.17352>, 2021.

948 Bréchet, L. M., Salomón, R. L., Machacova, K., Stahl, C., Burban, B., Goret, J. Y., Steppe, K., Damien, B.,
949 & Janssens, I. A.: Insights into the sub daily variations in methane, nitrous oxide and carbon
950 dioxide fluxes from upland tropical tree stems, *New Phytologist*, 20401,
951 <https://doi.org/10.1111/nph.20401>, 2025.

952 Brümmer, C., Falk, U., Papen, H., Szarzynski, J., Wassmann, R., & Brüggemann, N.: Diurnal, seasonal,
953 and interannual variation in carbon dioxide and energy exchange in shrub savanna in Burkina
954 Faso (West Africa), *Biogeosciences*, 113, G2030, <https://doi.org/10.1029/2007JG000583>, 2008.

955 Brümmer, C., Papen, H., Wassmann, R., & Brüggemann, N.: Fluxes of CH₄ and CO₂ from soil and
956 termite mounds in south Sudanian savanna of Burkina Faso (West Africa), *Global Biogeochemical*
957 *Cycles*, 23, GB1001, <https://doi.org/10.1029/2008GB003237>, 2009.

958 Cardinael, R., Cadisch, G., Gosme, M., Oelbermann, M., & Van Noordwijk, M.: Climate change
959 mitigation and adaptation in agriculture: Why agroforestry should be part of the solution? *Agr.*
960 *Ecosyst. Environ.*, 319, 107555, <https://doi.org/10.1016/j.agee.2021.107555>, 2021.

961 Charbonnier, F., Roupsard, O., le Maire, G., Guillemot, J., Casanoves, F., Lacoïnte, A., Vaast, P.,
962 Allinne, C., Audebert, L., Cambou, A., Clément-Vidal, A., Defrenet, E., Duursma, R. A., Jarri, L.,
963 Jourdan, C., Khac, E., Leandro, P., Medlyn, B. E., Saint-André, L., Thaler, P., Van Den Meersche, K.,
964 Barquero Aguilar, A., Lehner, P., & Dreyer, E.: Increased light-use efficiency sustains net primary
965 productivity of shaded coffee plants in agroforestry system, *Plant Cell and Environment*, 40(8),
966 1592-1608, <https://doi.org/10.1111/pce.12964>, 2017.

967 Chu, H., Luo, X., Ouyang, Z., et al.: Representativeness of Eddy-Covariance flux footprints for areas
968 surrounding AmeriFlux sites, *Agr. Forest. Meteorol.*, 301-302, 108350,
969 <https://doi.org/10.1016/j.agrformet.2021.108350>, 2021.

970 Clermont-Dauphin, C., N'dienor, M., Leroux, L., Ba, Halimatou. S., Bongers, F., Jourdan, C., Roupsard,
971 O., Do, F. C., Cournac, L., & Seghier, J.: *Faidherbia albida* trees form a natural buffer against millet
972 water stress in agroforestry parklands in Senegal, *Biotechnol. Agron. Soc. Environ*, 182-195,
973 <https://doi.org/10.25518/1780-4507.20477>, 2023.

974 Conant, R. T., Dalla-Betta, P., Klopatek, C. C., & Klopatek, J. M.: Controls on soil respiration in
975 semiarid soils, *Soil Biology and Biochemistry*, 36(6), 945-951,
976 <https://doi.org/10.1016/j.soilbio.2004.02.013>, 2004.

977 Crosson, E.: A cavity ring-down analyzer for measuring atmospheric levels of methane, carbon
978 dioxide, and water vapor, *App. Phys. B-Lasers O.*, 92, 403-408, [https://doi.org/10.1007/s00340-](https://doi.org/10.1007/s00340-008-3135-y)
979 [008-3135-y](https://doi.org/10.1007/s00340-008-3135-y), 2008.

980 de Carvalho, A. F., Fernandes-Filho, E. I., Daher, M., Gomes, L. de C., Cardoso, I. M., Fernandes, R. B.
981 A., & Schaefer, C. E. G. R.: Microclimate and soil and water loss in shaded and unshaded
982 agroforestry coffee systems, *Agroforest. Syst.*, 95(1), 119-134, [https://doi.org/10.1007/s10457-](https://doi.org/10.1007/s10457-020-00567-6)
983 [020-00567-6](https://doi.org/10.1007/s10457-020-00567-6), 2021.

984 Delon, C., Galy-Lacaux, C., Serça, D., Personne, E., Mougin, E., Adon, M., ... & Tagesson, T.: Modelling
985 land-atmosphere daily exchanges of NO, NH₃, and CO₂ in a semi-arid grazed ecosystem in Senegal,
986 *Biogeosciences*, 16(9), 2049-2077, <https://doi.org/10.5194/bg-16-2049-2019>, 2019.

987 Delaunay, V., Desclaux, A., & Sokhna, Ch.: Niakhar, mémoires et perspectives : Recherches
988 pluridisciplinaires sur le changement en Afrique, IRD Éditions/L'Harmattan, 536 p., ISBN
989 9782140103551, 2140103556 https://www.editions.ird.fr/open_access_download/851/441,
990 2019.

991 DeLucia, E. H., Drake, J. E., Thomas, R. B., & Gonzalez-Meler, M.: Forest carbon use efficiency: Is
992 respiration a constant fraction of gross primary production?, *Glob. Change Biol.*, 13(6),
993 1157-1167, <https://doi.org/10.1111/j.1365-2486.2007.01365.x>, 2007.

994 Denmead, O. T.: Approaches to measuring fluxes of methane and nitrous oxide between
995 landscapes and the atmosphere, *Plant and Soil*, 309(1-2), 5-24, [https://doi.org/10.1007/s11104-](https://doi.org/10.1007/s11104-008-9599-z)
996 [008-9599-z](https://doi.org/10.1007/s11104-008-9599-z), 2008.

997 Diack, I., Diene, S., Leroux, L., Diouf, A., Benjamin, H., Olivier, R., Letourmy, P., Alain, A., Sarr, I., &
998 Moussa, D.: Combining UAV and Sentinel-2 Imagery for Estimating Millet FCover in a
999 Heterogeneous Agricultural Landscape of Senegal, *IEEE Journal of Selected Topics in Applied*
1000 *Earth Observations and Remote Sensing*, 17, 7305-7322,
1001 <https://doi.org/10.1109/JSTARS.2024.3373508>, 2024.

1002 Diene, S. M., Diack, I., Audebert, A., Roupsard, O., Leroux, L., Diouf, A. A., Mbaye, M., Fernandez, R.,
1003 Diallo, M., Sarr, I.: Improving pearl millet yield estimation from UAV imagery in the semiarid
1004 agroforestry system of Senegal through textural indices and reflectance normalization, in *IEEE*
1005 *Access*, 12, 132626-132643, <https://doi.org/10.1109/ACCESS.2024.3460107>, 2024.

1006 Dilla, A. M., Smethurst, P. J., Barry, K., & Parsons, D.: Preliminary estimate of carbon sequestration
1007 potential of *Faidherbia albida* (Delile) A. Chev in an agroforestry parkland in the Central Rift Valley
1008 of Ethiopia, *Forests, Trees and Livelihoods*, 28(2), 79-89,
1009 <https://doi.org/10.1080/14728028.2018.1564146>, 2019.

1010 Diongue, D., Brunetti, G., Stumpp, C., Do, F., Roupsard, O., Orange, D., Faye, W., Sow, S., Jourdan, C.,
1011 & Faye, S.: A Probabilistic Framework for Assessing the Hydrological Impact of *Faidherbia Albida*
1012 in an Arid Area of Senegal, *Journal of Hydrology*, 622, 129717,
1013 <https://doi.org/10.1016/j.jhydrol.2023.129717>, 2023.

1014 Diongue, D. M. L., Roupsard, O., Do, F. C., Stumpp, C., Orange, D., Sow, S., Jourdan, C., & Faye, S.:
1015 Evaluation of parameterisation approaches for estimating soil hydraulic parameters with
1016 HYDRUS-1D in the groundnut basin of Senegal, *Hydrological Sciences Journal*, 67(15), 2327-
1017 2343, <https://doi.org/10.1080/02626667.2022.2142474>, 2022.

1018 Duthoit, M., Roupsard, O., Créquy, N., & Sauze, J.: Conception d'un dispositif automatisé de
1019 chambres de mesures d'échanges gazeux du sol à fermeture horizontale, *Le Cahier des Techniques*
1020 *de l'Inra*, 102, 19 p., hal-03989886, <https://hal.science/hal-03989886/document>, 2020.

- 1021 Eldridge, D.J., Ding, J., Dorrough, J. et al. Hotspots of biogeochemical activity linked to aridity and
1022 plant traits across global drylands. *Nat. Plants* 10, 760–770 (2024).
1023 <https://doi.org/10.1038/s41477-024-01670-7>
- 1024 Evans, S., Dieckmann, U., Franklin, O., & Kaiser, C.: Synergistic effects of diffusion and microbial
1025 physiology reproduce the Birch effect in a micro-scale model, *Soil Biology and Biochemistry*, 93,
1026 28-37, <https://doi.org/10.1016/j.soilbio.2015.10.020>, 2016.
- 1027 Falge, E., Baldocchi, D., Olson, R., Anthoni, P., Aubinet, M., Bernhofer, C., Burba, G., Ceulemans, R.,
1028 Clement, R., Dolman, H., Granier, A., Gross, P., Grünwald, T., Hollinger, D., Jensen, N.-O., Katul, G.,
1029 Keronen, P., Kowalski, A., Ta Lai, C., ... Oren, R.: Gap filling strategies for defensible annual sums of
1030 net ecosystem exchange, *Agr. Forest Meteorol.*, 107, 43-69, [https://doi.org/10.1016/S0168-](https://doi.org/10.1016/S0168-1923(00)00225-2)
1031 [1923\(00\)00225-2](https://doi.org/10.1016/S0168-1923(00)00225-2), 2001.
- 1032 Fan, Z., Neff, J. C., & Hanan, N. P.: Modeling pulsed soil respiration in an African savanna ecosystem,
1033 *Agr. Forest Meteorol.*, 200, 282-292, <https://doi.org/10.1016/j.agrformet.2014.10.009>, 2015.
- 1034 Fang, F., Han, X., Liu, W., & Tang, M.: Carbon dioxide fluxes in a farmland ecosystem of the southern
1035 Chinese Loess Plateau measured using a chamber-based method, *PeerJ*, 8, 8994,
1036 <https://doi.org/10.7717/peerj.8994>, 2020.
- 1037 Faye, W., Fall, A. N., Orange, D., Do, F., Roupsard, O., & Kane, A.: Climatic variability in the Sine-
1038 Saloum basin and its impacts on water resources: Case of the Sob and Diahine watersheds in the
1039 region of Niakhar, *Proceedings of the International Association of Hydrological Sciences*, 383,
1040 391-399, <https://doi.org/10.5194/piahs-383-391-2020>, 2020.
- 1041 Finkelstein, P. L., & Sims, P. F.: Sampling error in eddy correlation flux measurements, *J. Geophys.*
1042 *Res.*, 106(D4), 3503–3509, <https://doi.org/10.1029/2000JD900731>, 2001.
- 1043 Fleck, D., He, Y., Alexander, C., Jacobson, G., & Cunningham, K. L.: Simultaneous soil flux
1044 measurements of five gases-N₂O, CH₄, CO₂, NH₃, and H₂O-with the Picarro G2508," *Picarro*
1045 *Application Note*, AN034,
1046 [https://www.picarro.com/sites/default/files/product_documents/Picarro AN034 Soil%20Flux](https://www.picarro.com/sites/default/files/product_documents/Picarro_AN034_Soil%20Flux%20with%20the%20G2508_1.pdf)
1047 [%20with%20the%20G2508_1.pdf](https://www.picarro.com/sites/default/files/product_documents/Picarro_AN034_Soil%20Flux%20with%20the%20G2508_1.pdf), 2013.
- 1048 Foken, T., Göckede, M., Mauder, M., Mahrt, L., Amiro, B., Munger, W.: Post-Field Data Quality
1049 Control, In: Lee, X., Massman, W., Law, B. (eds) *Handbook of Micrometeorology*, *Atmos. Ocean. Sci.*
1050 *Lib.*, vol 29, Springer, Dordrecht, https://doi.org/10.1007/1-4020-2265-4_9, 2004.

1051 Foken, T., Aubinet, M., & Leuning, R.: Eddy Covariance. In M. Aubinet, T. Vesala, & D. Papale (eds),
1052 Eddy Covariance, p.1-19, Springer, Netherlands, <https://doi.org/10.1007/978-94-007-2351-1>,
1053 2012.

1054 Fox, J., Weisberg, S., & Price, B.: car: Companion to Applied Regression (version 3.1-3) [Dataset].
1055 <https://doi.org/10.32614/CRAN.package.car>, 2023.

1056 Gomes, L. D. C., Cardoso, I. M., Mendonça, E. D. S., Fernandes, R. B. A., Lopes, V. S., & Oliveira, T. S.:
1057 Trees modify the dynamics of soil CO₂ efflux in coffee agroforestry systems, *Agr. Forest. Meteorol.*,
1058 224, 30-39, <https://doi.org/10.1016/j.agrformet.2016.05.001>, 2016.

1059 Gonsamo, A., Chen, J. M., He, L., Sun, Y., Rogers, C., & Liu, J.: Exploring SMAP and OCO-2 observations
1060 to monitor soil moisture control on photosynthetic activity of global drylands and croplands,
1061 *Remote Sensing of Environment*, 232, 111314, <https://doi.org/10.1016/j.rse.2019.111314>, 2019.

1062 Guillen-Cruz, G., Campuzano, E. F., Juárez-Altamirano, R., López-García, K. L., Torres-Arreola, R., &
1063 Flores-Rentería, D.: Interannual Variation and Control Factors of Soil Respiration in Xeric
1064 Shrubland and Agricultural Sites from the Chihuahuan Desert, Mexico, *Land*, 12(11), 1961,
1065 <https://doi.org/10.3390/land12111961>, 2023.

1066 Gupta, S.R., Dagar, J.C., Sileshi, G.W., Chaturvedi, R.K.: Agroforestry for Climate Change Resilience
1067 in Degraded Landscapes. In: Dagar, J.C., Gupta, S.R., Sileshi, G.W. (eds) *Agroforestry for Sustainable*
1068 *Intensification of Agriculture in Asia and Africa*, Sustainability Sciences in Asia and Africa,
1069 Springer, Singapore. https://doi.org/10.1007/978-981-19-4602-8_5, 2023.

1070 Houghton, R. A. and Hackler, J. L.: Emissions of carbon from land use change in sub-Saharan Africa,
1071 *Geophys. Res.*, 111, G02003, <https://doi.org/10.1029/2005JG000076>, 2006.

1072 IUSS Working Group WRB.: World Reference Base for Soil Resources. International soil
1073 classification system for naming soils and creating legends for soil maps, 4th edition, International
1074 Union of Soil Sciences (IUSS), Vienna, Austria, ISBN 979-8-9862451-1-9,
1075 www.isric.org/sites/default/files/WRB_fourth_edition_2022-12-18.pdf, 2022.

1076 Jackson, R.B., Canadell, J., Ehleringer, J.R. et al.: A global analysis of root distributions for terrestrial
1077 biomes, *Oecologia* 108, 389–411, <https://doi.org/10.1007/BF00333714>, 1996.

1078 Jevon, F. V., Gewirtzman, J., Lang, A. K., Ayres, M. P., & Matthes, J. H.: Tree Species Effects on Soil
1079 CO₂ and CH₄ Fluxes in a Mixed Temperate Forest, *Ecosystems*, 26(7), 1587-1602,
1080 <https://doi.org/10.1007/s10021-023-00852-2>, 2023.

1081 Jia, X., Mu, Y., Zha, T., Wang, B., Qin, S., & Tian, Y.: Seasonal and interannual variations in ecosystem
1082 respiration in relation to temperature, moisture, and productivity in a temperate semi-arid
1083 shrubland, *Science of The Total Environment*, 709, 136210,
1084 <https://doi.org/10.1016/j.scitotenv.2019.136210>, 2020.

1085 Juszczak, R., Acosta, M., Olejnik, J.: Comparison of Daytime and Nighttime Ecosystem Respiration
1086 Measured by the Closed Chamber Technique on a Temperate Mire in Poland, *Pol. J. Environ. Stud.*
1087 Vol. 21, No. 3, 643-658, 2012.

1088 Kim, D. G., Vargas, R., Bond-Lamberty, B., & Turetsky, M. R.: Effects of soil rewetting and thawing
1089 on soil gas fluxes: A review of current literature and suggestions for future research,
1090 *Biogeosciences*, 9(7), 2459-2483, <https://doi.org/10.5194/bg-9-2459-2012>, 2012.

1091 Kim, D.-G., Thomas, A. D., Pelster, D., Rosenstock, T. S., & Sanz-Cobena, A.: Greenhouse gas
1092 emissions from natural ecosystems and agricultural lands in sub-Saharan Africa: Synthesis of
1093 available data and suggestions for further research, *Biogeosciences*, 13(16), 4789-4809,
1094 <https://doi.org/10.5194/bg-13-4789-2016>, 2016.

1095 Klaus, M., Öquist, M., & Macháčová, K.: Tree stem-atmosphere greenhouse gas fluxes in a boreal
1096 riparian forest, *Science of The Total Environment*, 954, 176243.
1097 <https://doi.org/10.1016/j.scitotenv.2024.176243>, 2024.

1098 Kormann, R., & Meixner, F. X.: An analytical footprint model for non-neutral stratification,
1099 *Boundary-Layer Meteorology*, 99, 207-224, <https://doi.org/10.1023/A:1018991015119>, 2001.

1100 Kuyah, S., Whitney, C. W., Jonsson, M., Sileshi, G. W., Öborn, I., Muthuri, C. W., & Luedeling, E.:
1101 Agroforestry delivers a win-win solution for ecosystem services in sub-Saharan Africa. A meta-
1102 analysis, *Agronomy for Sustainable Development*, 39(5), [https://doi.org/10.1007/s13593-019-](https://doi.org/10.1007/s13593-019-0589-8)
1103 [0589-8](https://doi.org/10.1007/s13593-019-0589-8), 2019.

1104 Lambers, H., Chapin, F. S., & Pons, T. L.: *Plant Physiological Ecology*, Springer New York.
1105 <https://doi.org/10.1007/978-0-387-78341-3>, 2008.

1106 Lasslop, G., Reichstein, M., Papale, D., Richardson, A., Arneth, A., Barr, A., Stoy, P., & Wohlfahrt, G.:
1107 Separation of net ecosystem exchange into assimilation and respiration using a light response
1108 curve approach: Critical issues and global evaluation, *Glob. Change Biol.*, 16(1), 187-208.
1109 <https://doi.org/10.1111/j.1365-2486.2009.02041.x>, 2010.

- 1110 Lembrechts J.J, Aalto J, Ashcroft MB, et al.: SoilTemp: A global database of near-surface
1111 temperature, *Glob. Change Biol.*, 26, 6616–6629, <https://doi.org/10.1111/gcb.15123>, 2020.
- 1112 Lembrechts, J. J., van den Hoogen, J., Aalto, J., et al.: Global maps of soil temperature. *Glob. Change*
1113 *Biol.*, 28, 3110-3144, <https://doi.org/10.1111/gcb.16060>, 2022.
- 1114 Leroux, L., Falconnier, G. N., Diouf, A. A., Ndao, B., Gbodjo, J. E., Tall, L., Balde, A. A., Clermont-
1115 Dauphin, C., Bégué, A., Affholder, F., & Rouspard, O.: Using remote sensing to assess the effect of
1116 trees on millet yield in complex parklands of Central Senegal, *Agr. Syst.*, 184,
1117 <https://doi.org/10.1016/j.agsy.2020.102918>, 2020.
- 1118 Liu, W., Zhang, Z., & Wan, S.: Predominant role of water in regulating soil and microbial respiration
1119 and their responses to climate change in a semiarid grassland, *Glob. Change Biol.*, 15(1), 184-195,
1120 <https://doi.org/10.1111/j.1365-2486.2008.01728.x>, 2009.
- 1121 Liu, Y., He, N., Wen, X., Xu, L., Sun, X., Yu, G., Liang, L., & Schipper, L. A.: The optimum temperature
1122 of soil microbial respiration: Patterns and controls, *Soil Biology and Biochemistry*, 121, 35-42,
1123 <https://doi.org/10.1016/j.soilbio.2018.02.019>, 2018.
- 1124 Lloyd, J., & Taylor, J. A.: On the Temperature Dependence of Soil Respiration, *Functional Ecology*,
1125 8(3), 315-323, <https://doi.org/10.2307/2389824>, 1994.
- 1126 Lopes, V. S., Cardoso, I. M., Cavalcante, V. S., Gomes, L. de C., Tanure, M. M. C., Moura, W. de M.,
1127 Mendonça, E. de S., & Fernandes, R. B. A.: Soil CO₂ efflux in coffee agroforestry and full-sun coffee
1128 systems, *Acta Sci. – Agr*, 46(1), e65877, <https://doi.org/10.4025/actasciagron.v46i1.65877>,
1129 2024.
- 1130 Lüdecke, D., Ben-Shachar, M., Patil, I., Waggoner, P., & Makowski, D.: Performance: An R Package
1131 for Assessment, Comparison and Testing of Statistical Models, *Journal of Open-Source Software*,
1132 6(60), 3139, <https://doi.org/10.21105/joss.03139>, 2021.
- 1133 Luo, Y., & Zhou, X.: Methods of Measurements and Estimations. In Y. Luo & X. Zhou (eds) *Soil*
1134 *Respiration and Environment*, 161-185 p., Academic Press, Elsevier,
1135 <https://doi.org/10.1016/B978-0-12-088782-8.X5000-1>, 2006.
- 1136 Macharia, J. M., Pelster, D. E., Ngetich, F. K., Shisanya, C. A., Mucheru-Muna, M., & Mugendi, D. N.:
1137 Soil greenhouse gas fluxes from maize production under different soil fertility management
1138 practices in East Africa, *Journal of Geophysical Research: Biogeosciences*, 125(7),
1139 e2019JG005427, <https://doi.org/10.1029/2019JG005427>, 2020.

- 1140 Malou, O. P., Moulin, P., Chevallier, T., Masse, D., Vayssières, J., Badiane-Ndour, N. Y., Tall, L., Thiam,
1141 A., & Chapuis-Lardy, L.: Estimates of carbon stocks in sandy soils cultivated under local
1142 management practices in Senegal's groundnut basin, *Regional Environmental Change*, 21(3), 65,
1143 <https://doi.org/10.1007/s10113-021-01790-2>, 2021.
- 1144 Manzoni, S., Chakrawal, A., Fischer, T., Schimel, J. P., Porporato, A., & Vico, G.: Rainfall
1145 intensification increases the contribution of rewetting pulses to soil heterotrophic respiration,
1146 *Biogeosciences*, 17(15), 4007-4023, <https://doi.org/10.5194/bg-17-4007-2020>, 2020.
- 1147 Mapanda, F., Mupini, J., Wuta, M., Nyamangara, J., & Rees, R. M.: A cross-ecosystem assessment of
1148 the effects of land cover and land use on soil emission of selected greenhouse gases and related
1149 soil properties in Zimbabwe, *European Journal of Soil Science*, 61(5), 721-733,
1150 <https://doi.org/10.1111/j.1365-2389.2010.01266.x>, 2010.
- 1151 Mazza, G., Agnelli, A. E., & Lagomarsino, A.: The effect of tree species composition on soil C and N
1152 pools and greenhouse gas fluxes in a Mediterranean reforestation, *Journal of Soil Science and Plant
1153 Nutrition*, 21(2), 1339-1352, <https://doi.org/10.1007/s42729-021-00444-w>, 2021.
- 1154 Mbow, C., Van Noordwijk, M., Luedeling, E., Neufeldt, H., Minang, P. A., & Kowero, G.: Agroforestry
1155 solutions to address food security and climate change challenges in Africa, *Current Opinion in
1156 Environmental Sustainability*, 6(1), 61-67, <https://doi.org/10.1016/j.cosust.2013.10.014>, 2014.
- 1157 Meena, A., Hanief, M., Dinakaran, J., & Rao, K. S.: Soil moisture controls the spatio-temporal pattern
1158 of soil respiration under different land use systems in a semi-arid ecosystem of Delhi, India,
1159 *Ecological Processes*, 9(1), 15, <https://doi.org/10.1186/s13717-020-0218-0>, 2020.
- 1160 Meisner, A., Rousk, J., & Bååth, E.: Prolonged drought changes the bacterial growth response to
1161 rewetting, *Soil Biology and Biochemistry*, 88, 314-322,
1162 <https://doi.org/10.1016/j.soilbio.2015.06.002>, 2015.
- 1163 Merbold, L., Ardo, J., Arneith, A., Scholes, R. J., Nouvellon, Y., de Grandcourt, A., Archibald, S.,
1164 Bonnefond, J. M., Boulain, N., Brueggemann, N., Bruemmer, C., Cappelaere, B., Ceschia, E., El-Khidir,
1165 H. A. M., El-Tahir, B. A., Falk, U., Lloyd, J., Kergoat, L., Le Dantec, V. L., Mougín, E., Muchinda, M.,
1166 Mukelabai, M. M., Ramier, D., Rounsard, O., Timouk, F., Veenendaal, E. M., & Kutsch, W. L.:
1167 Precipitation as driver of carbon fluxes in 11 African ecosystems, *Biogeosciences*, 6:1027-1041,
1168 <https://doi.org/10.5194/bg-6-1027-2009>, 2009.
- 1169 Moncrieff, J., Clement, R., Finnigan, J., Meyers, T.: Averaging, Detrending, and Filtering of Eddy
1170 Covariance Time Series. In: Lee, X., Massman, W., Law, B. (eds) *Handbook of Micrometeorology*,

1171 Atmos. Ocean. Sci. Lib., vol 29, Springer, Dordrecht, <https://doi.org/10.1007/1-4020-2265-4> 2,
1172 2004.

1173 Moncrieff, J. B., Massheder, J. M., De Bruin, H., Elbers, J., Friborg, T., Heusinkveld, B., Kabat, P., Scott,
1174 S., Soegaard, H., Verhoef, A.: A system to measure surface fluxes of momentum, sensible heat, water
1175 vapour and carbon dioxide, Journal of Hydrology, 188, 589-611, [https://doi.org/10.1016/S0022-
1176 1694\(96\)03194-0](https://doi.org/10.1016/S0022-1694(96)03194-0), 1997.

1177 Mosongo, P. S., Pelster, D. E., Li, X., Gaudel, G., Wang, Y., Chen, S., Li, W., Mburu, D., & Hu, C.:
1178 Greenhouse Gas Emissions Response to Fertilizer Application and Soil Moisture in Dry
1179 Agricultural Uplands of Central Kenya, Atmosphere, 13(3), 463,
1180 <https://doi.org/10.3390/atmos13030463>, 2022.

1181 Muggeo, V.M.R.: Estimating regression models with unknown break-points. Statist. Med., 22:
1182 3055-3071, <https://doi.org/10.1002/sim.1545>, 2003.

1183 Munjonji, L., Ntuli Innocentia, H., Ayisi, K. K., Dlamini, P., Mabitsela, K. E., Lehutjo, C. M., &
1184 Magnificent Zwane, P. S.: Seasonal dynamics of soil CO₂ emissions from different semi-arid land-
1185 use systems, Acta. Agr. Scand., Section BSP, 74(1), 2312934,
1186 <https://doi.org/10.1080/09064710.2024.2312934>, 2024.

1187 Nickerson, N. R.: Evaluating gas emission measurements using Minimum Detectable Flux (MDF),
1188 Eosene White papers, [https://eosense.com/wp-content/uploads/2019/11/Eosense-white-
1189 paper-Minimum-Detectable-Flux.pdf](https://eosense.com/wp-content/uploads/2019/11/Eosense-white-paper-Minimum-Detectable-Flux.pdf), 2016.

1190 Owusu-Prempeh, N., Amekudzi, L. K., & Kyereh, B.: Assessment of soil carbon dioxide efflux from
1191 contrasting land uses in a semi-arid savannah ecosystem, northeastern Ghana (West Africa),
1192 Scientific African, 26, e02420, <https://doi.org/10.1016/j.sciaf.2024.e02420>, 2024.

1193 Oyonarte, C., Rey, A., Raimundo, J., Miralles, I., & Escribano, P.: The use of soil respiration as an
1194 ecological indicator in arid ecosystems of the SE of Spain: Spatial variability and controlling
1195 factors, Ecological Indicators, 14(1), 40-49, <https://doi.org/10.1016/j.ecolind.2011.08.013>,
1196 2012.

1197 Padfield, D., Matheso, G., & Windram, F.: Package 'Nls. Multstart : Robust Non-Linear Regression
1198 using AIC Scores (R package version 2.0.0)', [DOI:10.32614/CRAN.package.nls.multstart,
1199 https://cran.r-project.org/web/packages/nls.multstart/nls.multstart.pdf](https://cran.r-project.org/web/packages/nls.multstart/nls.multstart.pdf), 2025.

1200 Pelster, D., Rufino, M., Rosenstock, T., Mango, J., Saiz, G., Diaz-Pines, E., Baldi, G., & Butterbach-Bahl,
1201 K., Smallholder farms in eastern African tropical highlands have low soil greenhouse gas fluxes,
1202 *Biogeosciences*, 14(1), 187-202, <https://doi.org/10.5194/bg-14-187-2017>, 2017.

1203 Picarro Inc.: PICARRO G2508 CRDS Analyzer N₂O + CH₄ + CO₂ + NH₃ + H₂O in Air, [Datasheet],
1204 [https://www.picarro.com/sites/default/files/product_documents/Picarro_G2508%20Analyzer](https://www.picarro.com/sites/default/files/product_documents/Picarro_G2508%20Analyzer%20Datasheet.pdf)
1205 [%20Datasheet.pdf](https://www.picarro.com/sites/default/files/product_documents/Picarro_G2508%20Analyzer%20Datasheet.pdf), 2015.

1206 Placella, S. A., Brodie, E. L., & Firestone, M. K.: Rainfall-induced carbon dioxide pulses result from
1207 sequential resuscitation of phylogenetically clustered microbial groups, *Proceedings of the*
1208 *National Academy of Sciences*, 109(27), 10931-10936,
1209 <https://doi.org/10.1073/pnas.1204306109>, 2012.

1210

1211 Pontauiller, J. Y., Hymus, G. J., & Drake, B. G.: Estimation of leaf area index using ground-based
1212 remote sensed NDVI measurements: Validation and comparison with two indirect techniques,
1213 *Canadian Journal of Remote Sensing*, 29(3), 381-387, <https://doi.org/10.5589/m03-009>, 2003.

1214 Poyda, A., Reinsch, T., Skinner, R. H., Kluß, C., Loges, R., & Taube, F.: Comparing chamber and eddy
1215 covariance based net ecosystem CO₂ exchange of fen soils; *Journal of Plant Nutrition and Soil*
1216 *Science*, 180(2), 252-266, <https://doi.org/10.1002/jpln.201600447>, 2017.

1217 Qiu, R., Han, G., Li, S., Tian, F., Ma, X., & Gong, W.: Soil moisture dominates the variation of gross
1218 primary productivity during hot drought in drylands, *Science of The Total Environment*, 899,
1219 165686, <https://doi.org/10.1016/j.scitotenv.2023.165686>, 2023.

1220 Quansah, E., Mauder, M., Balogun, A. A., Amekudzi, L. K., Hingerl, L., Bलिएfnicht, J., & Kunstmann,
1221 H.: Carbon dioxide fluxes from contrasting ecosystems in the Sudanian Savanna in West Africa,
1222 *Carbon Balance and Management*, 10(1), 1. <https://doi.org/10.1186/s13021-014-0011-4>, 2015.

1223 Rabbi, S. M. F., Warren, C., Swarbrick, B., Minasny, B., Mcbratney, A., & Young, I.: Microbial
1224 decomposition of organic matter and wetting-drying promotes aggregation in artificial soil but
1225 porosity increases only in wet-dry condition, *Geoderma*, 447, 116924,
1226 <https://doi.org/10.1016/j.geoderma.2024.116924>, 2024.

1227 Rahimi, J., Ago, E. E., Ayantunde, A., Berger, S., Bogaert, J., Butterbach-Bahl, K., Cappelaere, B.,
1228 Cohard, J.-M., Demarty, J., Diouf, A. A., Falk, U., Haas, E., Hiernaux, P., Kraus, D., Roupsard, O., Scheer,
1229 C., Srivastava, A. K., Tagesson, T., & Grote, R.: Modeling gas exchange and biomass production in

- 1230 West African Sahelian and Sudanian ecological zones, *Geoscientific Model Development*, 14(6),
1231 3789-3812, <https://doi.org/10.5194/gmd-14-3789-2021>, 2021.
- 1232 Raich, J. W., Lambers, H., & Oliver, D. J.: Respiration in Terrestrial Ecosystems, In D. M. Karl, & W.
1233 H., Schlesinger (Eds.), *Treatise on Geochemistry* (2 ed., Vol. 10, pp. 613-649), Elsevier,
1234 <https://doi.org/10.1016/B978-0-08-095975-7.00817-2>, 2014.
- 1235 Ramesh, T., Manjaiah, K. M., Tomar, J. M. S., & Ngachan, S. V.: Effect of multipurpose tree species on
1236 soil fertility and CO₂ efflux under hilly ecosystems of Northeast India, *Agr. Syst.*, 87(6), 1377-1388,
1237 <https://doi.org/10.1007/s10457-013-9645-6>, 2013.
- 1238 R. Core Team.: R: A language and environment for statistical computing, R Foundation for
1239 Statistical Computing, Vienna, Austria, 2023.
- 1240 Reichle, D. E.: Energy flow in ecosystems., In D.E. Reichle (ed) *The Global Carbon Cycle and Climate*
1241 *Change* (p. 119-156), Elsevier, <https://doi.org/10.1016/B978-0-12-820244-9.00008-1>, (2020).
- 1242 Reichstein, M., et al.: Modeling temporal and large-scale spatial variability of soil respiration from
1243 soil water availability, temperature and vegetation productivity indices, *Global Biogeochem.*
1244 *Cycles*, 17, 1104, doi:[10.1029/2003GB002035](https://doi.org/10.1029/2003GB002035), 4, 2003.
- 1245 Reichstein, M., Falge, E., Baldocchi, D., Papale, D., Aubinet, M., Berbigier, P., Bernhofer, C.,
1246 Buchmann, N., Gilmanov, T., Granier, A., Grünwald, T., Havránková, K., Ilvesniemi, H., Janous, D.,
1247 Knohl, A., Laurila, T., Lohila, A., Loustau, D., Matteucci, G., ... Valentini, R.: On the separation of net
1248 ecosystem exchange into assimilation and ecosystem respiration: Review and improved
1249 algorithm, *Glob. Change Biol.*, 11(9), 1424-1439, [https://doi.org/10.1111/j.1365-](https://doi.org/10.1111/j.1365-2486.2005.001002.x)
1250 [2486.2005.001002.x](https://doi.org/10.1111/j.1365-2486.2005.001002.x), 2005.
- 1251 Reum, F., Gerbig, C., Lavric, J. V., Rella, C. W., & Göckede, M.: Correcting atmospheric CO₂ and CH₄
1252 mole fractions obtained with Picarro analyzers for sensitivity of cavity pressure to water vapor,
1253 *Atmos. Meas. Tech.*, 12(2), 1013-1027, <https://doi.org/10.5194/amt-12-1013-2019>, 2005.
- 1254 Rheault, K., Riis Christiansen, J., & Steenberg Larsen, K.: The role of tree species and microbes for
1255 the development of net greenhouse gas fluxes from soils after afforestation of agricultural lands,
1256 EGU General Assembly 2024, Vienna, Austria, 14-19 April 2024, EGU24-9718,
1257 <https://doi.org/10.5194/egusphere-egu24-9718>, 2024.

- 1258 Richardson, J., Chatterjee, A., & Darrel Jenerette, G.: Optimum temperatures for soil respiration
1259 along a semi-arid elevation gradient in southern California, *Soil Biology and Biochemistry*, 46,
1260 89-95, <https://doi.org/10.1016/j.soilbio.2011.11.008>, 2012.
- 1261 Riederer, M., Serafimovich, A., & Foken, T.: Net ecosystem CO₂ exchange measurements by the
1262 closed chamber method and the eddy covariance technique and their dependence on atmospheric
1263 conditions, *Atmos. Meas. Tech.*, 7(4), 1057-1064, <https://doi.org/10.5194/amt-7-1057-2014>,
1264 2014.
- 1265 Roby, M. C., Scott, R. L., Biederman, J. A., Smith, W. K., & Moore, D. J. P.: Response of soil carbon
1266 dioxide efflux to temporal repackaging of rainfall into fewer, larger events in a semiarid grassland,
1267 *Frontiers in Environmental Science*, 10. <https://doi.org/10.3389/fenvs.2022.940943>, 2022.
- 1268 Rolo, V., Rivest, D., Maillard, É., & Moreno, G.: Agroforestry potential for adaptation to climate
1269 change: A soil-based perspective, *Soil Use and Management*, 39(3), 1006-1032,
1270 <https://doi.org/10.1111/sum.12932>, 2023.
- 1271 Rong, Y., Ma, L., Johnson, D., & Yuan, F.: Soil respiration patterns for four major land-use types of
1272 the agro-pastoral region of northern China, *Agr. Ecosyst Environ.*, 213, 142-150,
1273 <https://doi.org/10.1016/j.agee.2015.08.002>, 2015.
- 1274 Rosenstock, T. S., Mpanda, M., Pelster, D. E., Butterbach-Bahl, K., Rufino, M. C., Thiong'o, M., Mutuo,
1275 P., Abwanda, S., Rioux, J., Kimaro, A. A., & Neufeldt, H.: Greenhouse gas fluxes from agricultural
1276 soils of Kenya and Tanzania: GHG Fluxes From Agricultural Soils of East Africa, *Journal of*
1277 *Geophysical Research: Biogeosciences*, 121(6), 1568-1580,
1278 <https://doi.org/10.1002/2016JG003341>, 2016.
- 1279 Rouspard, O., Ferhi, A., Granier, A., Pallo, F., Depommier, D., Mallet, B., Joly, H. I., & Dreyer, E.:
1280 Reverse Phenology and Dry-Season Water Uptake by *Faidherbia albida* (Del.) A. Chev. in an
1281 Agroforestry Parkland of Sudanese West Africa, *Functional Ecology*, 13(4), 460-472,
1282 <http://www.jstor.org/stable/2656552>, 1999.
- 1283 Rouspard, O., Audebert, A., Ndour, A. P., Clermont-Dauphin, C., Agbohessou, Y., Sanou, J., Koala, J.,
1284 Faye, E., Sambakhe, D., Jourdan, C., le Maire, G., Tall, L., Sanogo, D., Seghieri, J., Cournac, L., & Leroux,
1285 L.: How far does the tree affect the crop in agroforestry? New spatial analysis methods in a
1286 *Faidherbia parkland*, *Agr. Ecosyst. Environ.*, 296, 106928,
1287 <https://doi.org/10.1016/j.agee.2020.106928>, 2020.

- 1288 Sarr, M.S., Diouf D., Roupsard O., Rocheteau A., Orange D., et al.: Estimation of seasonal water use
1289 of *Faidherbia albida* (Delile) A.Chev. in a Sahelian agroforestry parkland, *Biotechnol. Agron. Soc.*
1290 *Environ.*, 27(3), 196-204, <https://doi.org/10.25518/1780-4507.20512>, 2023.
- 1291 Schimel, J., Balser, T. C., & Wallenstein, M.: Microbial stress-response physiology and its
1292 implications for ecosystem function, *Ecology*, 88(6), 1386-1394, [https://doi.org/10.1890/06-](https://doi.org/10.1890/06-0219)
1293 [0219](https://doi.org/10.1890/06-0219), 2007.
- 1294 Sida, T. S., Baudron, F., Kim, H., & Giller, K. E.: Climate-smart agroforestry: *Faidherbia albida* trees
1295 buffer wheat against climatic extremes in the Central Rift Valley of Ethiopia, *Agr. Forest Meteorol.*,
1296 248, 339-347, <https://doi.org/10.1016/j.agrformet.2017.10.013>, 2018.
- 1297 Siegwart, L., Bertrand, I., Roupsard, O., Duthoit, M., & Jourdan, C.: Root litter decomposition in a
1298 sub-Saharan agroforestry parkland dominated by *Faidherbia albida*, *Journal of Arid*
1299 *Environments*, 198, 104696, <https://doi.org/10.1016/j.jaridenv.2021.104696>, 2022.
- 1300 Siegwart, L., Bertrand, I., Roupsard, O., & Jourdan, C.: Contribution of tree and crop roots to soil
1301 carbon stocks in a Sub-Saharan agroforestry parkland in Senegal, *Agr. Ecosyst. Environ.*, 352,
1302 108524, <https://doi.org/10.1016/j.agee.2023.108524>, 2023.
- 1303 Sileshi, G. W.: The magnitude and spatial extent of influence of *Faidherbia albida* trees on soil
1304 properties and primary productivity in drylands, *Journal of Arid Environments*, 132, 1-14,
1305 <https://doi.org/10.1016/j.jaridenv.2016.03.002>, 2016.
- 1306 Sileshi, G. W., Teketay, D., Gebrekirstos, A., & Hadgu, K.: Sustainability of *Faidherbia albida*-Based
1307 Agroforestry in Crop Production and Maintaining Soil Health., In J. C. Dagar, S. R. Gupta, & D.
1308 Teketay (eds), *Agroforestry for Degraded Landscapes: Recent Advances and Emerging*
1309 *Challenges—Vol. 2* (p. 349-369), Springer Singapore, [https://doi.org/10.1007/978-981-15-](https://doi.org/10.1007/978-981-15-6807-7_12)
1310 [6807-7_12](https://doi.org/10.1007/978-981-15-6807-7_12), 2020.
- 1311 Singh, S., Mayes, M., Kivlin, S., & Jagadamma, S.: How the Birch Effect differs in mechanisms and
1312 magnitudes due to soil texture, *Soil Biology and Biochemistry*, 179, 108973,
1313 <https://doi.org/10.1016/j.soilbio.2023.108973>, 2023.
- 1314 Soudani, K., Hmimina, G., Delpierre, N., Pontailier, J. Y., Aubinet, M., Bonal, D., Caquet, B., de
1315 Grandcourt, A., Burban, B., Flechard, C., Guyon, D., Granier, A., Gross, P., Heinesh, B., Longdoz, B.,
1316 Loustau, D., Moureaux, C., Ourcival, J. M., Rambal, S., Saint André.L, Dufrene, E.: Ground-based
1317 Network of NDVI measurements for tracking temporal dynamics of canopy structure and

1318 vegetation phenology in different biomes, *Remote Sensing of Environment*, 123, 234-245,
1319 <https://doi.org/10.1016/j.rse.2012.03.012>, 2012.

1320 Skinner, R. H., & Wagner-Riddle, C.: Micrometeorological Methods for Assessing Greenhouse Gas
1321 Flux., In M. A. Liebig, A. J. Franzluebbers, & R. F. Follett (eds) *Managing Agricultural Greenhouse*
1322 *Gases: Coordinated Agricultural Research through GRACEnet to Address our Changing Climate* (p.
1323 367-383), Elsevier, <https://doi.org/10.1016/B978-0-12-386897-8.00021-8>, 2012.

1324 Stephen, E. A., Evans, K. D., & Akwasi, A. A.: Effects of *Faidherbia albida* on some important soil
1325 fertility indicators on agroforestry parklands in the semi-arid zone of Ghana, *Afr. J. Agr. Res.*,
1326 15(2), 256-268, <https://doi.org/10.5897/ajar2019.14617>, 2020.

1327 Stetter, C., & Sauer, J.: Tackling climate change: Agroforestry adoption in the face of regional
1328 weather extremes, *Ecological Economics*, 224, 108266,
1329 <https://doi.org/10.1016/j.ecolecon.2024.108266>, 2024.

1330 Stojanović, M., Jocher, G., Kowalska, N., Szatniewska, J., Zavadilová, I., Urban, O., Čáslavský, J.,
1331 Horáček, P., Acosta, M., Pavelka, M., & Marshall, J. D.: Disaggregation of canopy photosynthesis
1332 among tree species in a mixed broadleaf forest, *Tree Physiology*, 44(7), tpae064,
1333 <https://doi.org/10.1093/treephys/tpae064>, 2024.

1334 Tagesson, T., Ardö, J., Guiro, I., Cropley, F., Mbow, C., Horion, S., Ehammer, A., Mougín, E., Delon, C.,
1335 Galy-Lacaux, C., & Fensholt, R.: Very high CO₂ exchange fluxes at the peak of the rainy season in a
1336 West African grazed semi-arid savanna ecosystem, *Geografisk Tidsskrift - Danish Journal of*
1337 *Geography*, 116(a), 93-109, <https://doi.org/10.1080/00167223.2016.1178072>, 2016.

1338 Tagesson, T., Fensholt, R., Cappelaere, B., Mougín, E., Horion, S., Kergoat, L., Nieto, H., Mbow, C.,
1339 Ehammer, A., Demarty, J., & Ardö, J.: Spatiotemporal variability in carbon exchange fluxes across
1340 the Sahel, *Agr. Forest Meteorol.*, 226-227(b), 108-118,
1341 <https://doi.org/10.1016/j.agrformet.2016.05.013>, 2016.

1342 Tagesson, T., Fensholt, R., Cropley, F., Guiro, I., Horion, S., Ehammer, A., & Ardö, J.: Dynamics in
1343 carbon exchange fluxes for a grazed semi-arid savanna ecosystem in West Africa. *Agr. Ecosyst.*
1344 *Environ.*, 205, 15-24, <https://doi.org/10.1016/j.agee.2015.02.017>, 2015.

1345 Tang, J., Bolstad, P. V., Desai, A. R., Martin, J. G., Cook, B. D., Davis, K. J., & Carey, E. V.: Ecosystem
1346 respiration and its components in an old-growth forest in the Great Lakes region of the United
1347 States, *Agr. Forest Meteorol.*, 148(2), 171-185, <https://doi.org/10.1016/j.agrformet.2007.08.008>,
1348 2008.

- 1349 Tang, X., Carvalhais, N., Moura, C., Ahrens, B., Koirala, S., Fan, S., Guan, F., Zhang, W., Gao, S.,
1350 Magliulo, V., Buysse, P., Liu, S., Chen, G., Yang, W., Yu, Z., Liang, J., Shi, L., Pu, S., & Reichstein, M.:
1351 Global variability of carbon use efficiency in terrestrial ecosystems, *Biogeochemistry: Land*,
1352 <https://doi.org/10.5194/bg-2019-37>, 2019.
- 1353 Tucker, C. L., & Reed, S. C.: Low soil moisture during hot periods drives apparent negative
1354 temperature sensitivity of soil respiration in a dryland ecosystem: A multi-model comparison,
1355 *Biogeochemistry*, 128(1-2), 155-169, <https://doi.org/10.1007/s10533-016-0200-1>, 2016.
- 1356 Unger, S., Máguas, C., Pereira, J. S., David, T. S., & Werner, C.: The influence of precipitation pulses
1357 on soil respiration – Assessing the “Birch effect” by stable carbon isotopes, *Soil Biology and*
1358 *Biochemistry*, 42(10), 1800-1810, <https://doi.org/10.1016/j.soilbio.2010.06.019>, 2010.
- 1359 Valujeva, K., Pilecka-Ulcugaceva, J., Skiste, O., Liepa, S., Lagzdins, A., & Grinfelde, I.: Soil tillage and
1360 agricultural crops affect greenhouse gas emissions from Cambic Calcisol in a temperate climate,
1361 *Acta. Agr. Scand. B-S-P.*, 72(1), 835-846, <https://doi.org/10.1080/09064710.2022.2097123>,
1362 2022.
- 1363 Van Haren, J. L. M., De Oliveira, R. C., Restrepo-Coupe, N., Hutrya, L., De Camargo, P. B., Keller, M.,
1364 & Saleska, S. R.: Do plant species influence soil CO₂ and N₂ O fluxes in a diverse tropical forest?
1365 *Journal of Geophysical Research: Biogeosciences*, 115, G03010,
1366 <https://doi.org/10.1029/2009JG001231>, 2010.
- 1367 Vargas, R., Enrique, S. C. P., Serrano-Ortiz, P., Yuste, J. C., Domingo, F., López-Ballesteros, A., &
1368 Oyonarte, C.: Hot-moments of soil CO₂ efflux in a water-limited grassland, *Soil Systems*, 2(3), 1-18,
1369 <https://doi.org/10.3390/soilsystems2030047>, 2018.
- 1370 Vickers, D., & Mahrt, L.: Quality Control and Flux Sampling Problems for Tower and Aircraft Data,
1371 *Journal of Atmospheric and Oceanic Technology*, 14(3), 512-526,
1372 [http://dx.doi.org/10.1175/1520-0426\(1997\)014%3C0512:QCAFSP%3E2.0.CO;2](http://dx.doi.org/10.1175/1520-0426(1997)014%3C0512:QCAFSP%3E2.0.CO;2), 1997.
- 1373 Wachiye, S., Merbold, L., Vesala, T., Rinne, J., Räsänen, M., Leitner, S., & Pellikka, P.: Soil greenhouse
1374 gas emissions under different land-use types in savanna ecosystems of Kenya, *Biogeosciences*,
1375 17(8), 2149-2167, <https://doi.org/10.5194/bg-17-2149-2020>, 2020.
- 1376 Wang, M., Guan, D.-X., Han, S.-J., & Wu, J.-L.: Comparison of eddy covariance and chamber-based
1377 methods for measuring CO₂ flux in a temperate mixed forest, *Tree Physiology*, 30(1), 149-163,
1378 <https://doi.org/10.1093/treephys/tpp098>, 2010.

1379 Wang, Z., Ji, L., Hou, X., & Schellenberg, M. P.: Soil Respiration in Semiarid Temperate Grasslands
1380 under Various Land Management, PLOS ONE, 11(1), e0147987,
1381 <https://doi.org/10.1371/journal.pone.0147987>, 2016.

1382 Waring E., Quinn M., McNamara A., Arino de la Rubia E., Zhu H., Ellis S.: skimr: Compact and
1383 Flexible Summaries of Data, R package (version 2.1.5), <https://github.com/ropensci/skimr/>,
1384 <https://docs.ropensci.org/skimr/> (website), 2024.

1385 Warren, C. R. Response of osmolytes in soil to drying and rewetting. *Soil Biology and Biochemistry*,
1386 70, 22-32, <https://doi.org/10.1016/j.soilbio.2013.12.008>, 2014.

1387 Webb, E. K., Pearman, G. I., & Leuning, R., Correction of flux measurements for density effects due
1388 to heat and water vapour transfer. *Q. J. R. Meteorol. Soc.*, 106, 85-100,
1389 <https://doi.org/10.1002/qj.49710644707>, 1980.

1390 Wieckowski, A., Vestin, P., Ardö, J., Roupsard, O., Ndiaye, O., Diatta, O., Ba, S., Agbohessou, Y.,
1391 Fensholt, R., Verbruggen, W., Gebremedhn, H. H., & Tagesson, T.: Eddy covariance measurements
1392 reveal a decreased carbon sequestration strength 2010–2022 in an African semiarid savanna,
1393 *Glob. Change Biol.*, 30(9), e17509. <https://doi.org/10.1111/gcb.17509>, 2024.

1394 Wiesner, S., Desai, A. R., Duff, A. J., Metzger, S., & Stoy, P. C.: Quantifying the natural climate solution
1395 potential of agricultural systems by combining eddy covariance and remote sensing. *Journal of*
1396 *Geophysical Research: Biogeosciences*, 127(9), e2022JG006895,
1397 <https://doi.org/10.1029/2022JG006895>, 2022.

1398 Wild, J., Kopecký, M., Macek, M., Šanda, M., Jankovec, J., & Haase, T.: Climate at ecologically relevant
1399 scales: A new temperature and soil moisture logger for long-term microclimate measurement,
1400 *Agr. Forest Meteorol.*, 268, 40-47, <https://doi.org/10.1016/j.agrformet.2018.12.018>, 2019.

1401 Williams, C.A., Hanan, N.P., Neff, J.C. et al.: Africa and the global carbon cycle, *Carbon Balance*
1402 *Manage*, 2, 3, <https://doi.org/10.1186/1750-0680-2-3>, 2007.

1403 Williams, C. A., Hanan, N., Scholes, R. J., & Kutsch, W.: Complexity in water and carbon dioxide
1404 fluxes following rain pulses in an African savanna, *Oecologia*, 161(3), 469-480,
1405 <https://doi.org/10.1007/s00442-009-1405-y>, 2009.

1406 Wohlfahrt, G., & Galvagno, M.: Revisiting the choice of the driving temperature for eddy covariance
1407 CO₂ flux partitioning, *Agr. Forest Meteorol.*, 237-238, 135-142,
1408 <https://doi.org/10.1016/j.agrformet.2017.02.012>, 2017.

1409 Wutzler, T., Lucas-Moffat, A., Migliavacca, M., Knauer, J., Sickel, K., Šigut, L., Menzer, O., and
1410 Reichstein, M.: Basic and extensible post-processing of eddy covariance flux data with REddyProc,
1411 Biogeosciences, 15, 5015–5030, <https://doi.org/10.5194/bg-15-5015-2018>, 2018.

1412 Xenakis, G.: FREddyPro: Post-Processing EddyPro Full Output File. Edinburgh, UK. R package
1413 version 1.0.1., 2016.

1414 Xue, H., & Tang, H.: Responses of soil respiration to soil management changes in an agropastoral
1415 ecotone in Inner Mongolia, China, Ecology and Evolution, 8(1), 220-230,
1416 <https://doi.org/10.1002/ece3.3659>, 2018.

1417 Yan, L., Chen, S., Xia, J., & Luo, Y.: Precipitation regime shift enhanced the rain pulse effect on soil
1418 respiration in a semi-arid steppe, PLoS ONE, 9(8),
1419 <https://doi.org/10.1371/journal.pone.0104217>, 2014.

1420 Yu, H., Xu, Z., Zhou, G., & Shi, Y.: Soil carbon release responses to long-term versus short-term
1421 climatic warming in an arid ecosystem, Biogeosciences, 17(3), 781-792,
1422 <https://doi.org/10.5194/bg-17-781-2020>, 2020.

1423 Yu, T., Jiapaer, G., Bao, A., Zheng, G., Zhang, J., Li, X., Yuan, Y., Huang, X., & Umuhoza, J.: Disentangling
1424 the relative effects of soil moisture and vapor pressure deficit on photosynthesis in dryland
1425 Central Asia, Ecological Indicators, 137, 108698, <https://doi.org/10.1016/j.ecolind.2022.108698>,
1426 2022.

1427 Yu, X., Zha, T., Pang, Z., Wu, B., Wang, X., Chen, G., Li, C., Cao, J., Jia, G., Li, X., & Wu, H.: Response of
1428 soil respiration to soil temperature and moisture in a 50-year-old oriental arborvitae plantation
1429 in China, PLoS ONE, 6(12), <https://doi.org/10.1371/journal.pone.0028397>, 2011.

1430 Zaman M., Kleineidam K., Bakken L., Berendt J., Bracken C., Butterbach-Bahl K., Cai Z., Chang S. X.,
1431 Clough T., Dawar K., Ding W. X., Dörsch P., dos Reis Martins M., Eckhardt C., Fiedler S., Frosch T.,
1432 Goopy J., Görres C.-M., Gupta A., Henjes S., Hofmann M. E. G., Horn M. A., Jahangir M. M. R., Jansen-
1433 Willems A., Lenhart K., Heng L., Lewicka-Szczebak D., Lucic G., Merbold L., Mohn J., Molstad L.,
1434 Moser G., Murphy P., Sanz-Cobena A., Šimek M., Urquiaga S., Well R., Wrage-Mönnig N., Zaman S.,
1435 Zhang J., Müller C.: Greenhouse Gases from Agriculture. In M. Zaman, L. Hang, C. Müller (eds)
1436 Measuring emission of agricultural greenhouse gases and developing mitigation options using
1437 nuclear and related techniques Springer, Cham, https://doi.org/10.1007/978-3-030-55396-8_1,
1438 2021.

- 1439 Zeileis, A., Grothendieck, G., Ryan, J. A., Ulrich, J. M., & Andrews, F.: Package 'zoo': S3 Infrastructure
1440 for Regular and Irregular Time Series (Z's Ordered Observations) (version 1.8-12) [R Package],
1441 <https://zoo.R-Forge.R-project.org/>, 2024.
- 1442 Zhang, X., Bi, J., Zhu, D., & Meng, Z.: Seasonal variation of net ecosystem carbon exchange and gross
1443 primary production over a Loess Plateau semi-arid grassland of northwest China, *Scientific*
1444 *Reports*, 14(1), 2916, <https://doi.org/10.1038/s41598-024-52559-6>, 2024.
- 1445 Zhang, X., Ramakanth, K. K., & Long, Y.: The biomechanics of turgor pressure, *Current Biology*,
1446 34(20), R986-R991, <https://doi.org/10.1016/j.cub.2024.07.013>, 2024.
- 1447 Zhao, C., Miao, Y., Yu, C., Zhu, L., Wang, F., Jiang, L., Hui, D., & Wan, S.: Soil microbial community
1448 composition and respiration along an experimental precipitation gradient in a semiarid steppe,
1449 *Scientific Reports*, 6(1), 24317, <https://doi.org/10.1038/srep24317>, 2016.
- 1450 Zhou, Y., Williams, C. A., Lauvaux, T., Feng, S., Baker, I. T., Wei, Y., Denning, A. S., Keller, K., & Davis,
1451 K. J.: ACT-America: Gridded Ensembles of Surface Biogenic Carbon Fluxes, 2003-2019 (Version
1452 1.1), ORNL Distributed Active Archive Center, <https://doi.org/10.3334/ORNLDAAAC/1675>, 2019.
- 1453 Zhou, Y., Williams, C. A., Lauvaux, T., Davis, K. J., Feng, S., Baker, I., et al.: A multiyear gridded data
1454 ensemble of surface biogenic carbon fluxes for North America: Evaluation and analysis of results,
1455 *Journal of Geophysical Research: Biogeosciences*, 125, e2019JG005314,
1456 <https://doi.org/10.1029/2019JG005314>, 2020.